ADDIS ABABA INSTITUTE OF TECHNOLOGY
SCHOOL OF MULTI-DISCIPILNARY ENGINEERING
CENTER FOR MATERIALS ENGINEERING

Synthesis of High Refractive Index La^{3+} doped $BaTiO_3$ Nanoparticles for Retroreflective Application Via Water Assisted Solid State Reaction

By Hailu Redae

A Thesis Submitted to Addis Ababa Institute of Technology, School of Multi-Disciplinary Engineering, Center For Materials Engineering in Partial Fulfillment of the Degree of Master of Science in Materials Engineering

Addis Ababa, Ethiopia

June, 2019

Abstract

To guarantee the safe and well-organized movement of traffic on highway during bad weather and nighttime conditions, traffic signs, markings, helmet and safety textile paints have to be illuminated and made of retro-reflective materials. Materials having collective fluorescent and retro-reflective properties importantly improve visibility. For production of these materials Ceramics of glass having high refractive index are used.

Most ceramic materials for different applications are synthesized by a conventional solid state reaction (SSR) method. In solid state reaction ionic diffusion in an ionic crystal is very sluggish at about room temperature Therefore it needs a high temperature conditions for boosting the reactivity between raw materials. Liquid phase reaction also can arise at relatively low temperature to SSR but needs additional temperature to dry the solvent and superior equipment for separation. Methods currently used to synthesis glass beads such as Container less flame-spray, Conventional SSR, Molten salt etc. requires high temperature (780 ºC-1300ºC) to synthesize high purity glass beads. Furthermore, products obtained using these methods have large bead/ powder sizes.

In this study, a WASSR route is employed to synthesize nano-sized La^{3+} activated $BaTiO_3$ at 100ºc. The starting materials, La_2O_3, TiO_2, and Ba(OH)2.8H2O, weighed according to the stoichiometric ratio and mixed for 15 minutes with 8% of deionized water, Store in an automatic Oven for 6 hours at 100ºc. The La doping level were 0%, 5% and 10%.

X-ray diffraction of the as prepared new material confirmed the product has a structure of Tetragonal $BaTiO_3$ having a size ranging from 19.39 to 21.64nm.EDS mapping of the as prepared sample showed uniform distribution of components. From UV-Vi spectrometry, the La^{3+} activated $BaTiO_3$ nanoparticles has shown a refractive index of 3.392 when La doping was 1%. Raman spectroscopy also confirmed the structure of the as prepared sample is Tetragonal. The refractive index of nanoparticles greatly increased the wide wavelength range (426–900 nm), which is very useful for some special surfaces that require illumination from reflection of light rays, such as protective reflective helmet or clothes, road side signs, etc. In addition, it can be used as heat reflective layer, which solves the urban heat island effect.

ACKNOWLDGMENT

Special thanks go to Professor Byeong Soo LIM, a pioneer who opens up the Center for Materials Engineering and for his peerless contributions.

This thesis is not possible without the support from the following people and institutions. I heartily acknowledge Dr. Sintayehu Nibret (Assistant Professor) ,Yonas Asefa and Mr. Gueshe G/Mariam. Dr. Sintayehu Nibret and Yonas Asefa supported me to get characterization facilities to characterize samples at Sungkyunkwan University, South Korea. Mr. Gueshe G/Mariam is also acknowledged for his time and financial support including importing the starting materials, La_2O_3 and TiO_2, from Skyspring Nanomaterials Inc., Houston, U.S.A.

Thanks must also go to Dr. Anteneh Marelign (Assistant Professor) and Dr. Georgies Alene (Assistant Professor). I really appreciate their insightful guidance, invaluable advice, and continuous encouragement and support throughout the thesis work.

In addition, the staffs of Adama Science and Technology University in the Department of Materials Science and engineering are acknowledged for allowing and helping me in preparing materials and x-ray diffraction measurements.

I also would like to express my gratefulness to my families for their endless support, without which I could not complete my study. I also would like to thank W/ro Lemlem Fekadu, School Administrator at School of Multidisciplinary Engineering. Finally, I greatly thank all the students in our center, Center for Materials Engineering, for their valuable support.

TABLE OF CONTENTS

LIST OF TABLES

LIST OF FIGURES

LIST OF ABBREVIATIONS AND ACRONYMS

SSR	Solid-state reaction
WASSR	Water assisted solid state reaction
TEM	Transmission electron microscopy
SEM	Scanning electron microscopy
XRD	X-Ray diffraction
ICDD	International Center for Diffraction Data
EDS	Energy-dispersive X-ray spectroscopy
NPs	Nanoparticles
PL	Photoluminescence
PLE	Photoluminescence excitation
RBS	Rutherford back-scattering spectroscopy
XPS	X-Ray photoelectron spectroscopy
WAXS	Wide-angle X-ray Scattering
EXAFS	Extended X-Ray absorption fine structure

1. Introduction

1.1. Background

Ceramics of glass microspheres having high reflective index are used to produce high reflective coating, reflective pigment, reflective sheets, roadside signs, etc., and as a whole these micro-spheres are valuable related with any surface that needs illumination from reflection of light rays[1]. In addition, reflective materials can enhance detection in measurement systems and operate as reflecting units in optical communication equipment[2].Materials having collective fluorescent and retro-reflective properties importantly improve visibility, conspicuity of traffic signs and peoples working on road under all driving situations, suitable and bad weather. Retro-reflectivity is a property of a surface that allows a large portion of the light coming from a point source to be returned directly back to a point near its origin. During night time driver's vehicle headlamp is the sources of light basis of illumination for the roadway situations[3].

Road traffic safety is important to reduce the harms (deaths, injuries, and property damage) resulting from crashes of road vehicles traveling on public roads. Main goal of road traffic safety is protection and security of all those who travel on roads. Major factors that contribute to the road traffic safety can be grouped in three categories: Roads, Vehicles, Drivers' behavior. Road markings can be defined as a set of longitudinal and transversal lines, signs and symbols which combined form the surface transportation infrastructure. They represent part of the overall traffic signals and cannot be replaced by other signs or regulations. Road markings have the same legal value as the traffic signs and traffic light signals and can be set independently or in combination with them. The main tasks of the road markings are warning drivers about the situation in the area in front of vehicles that require special attention and caution for the continuation of safe driving, guiding the drivers to their targets by identifying safe travel path, inform drivers about the legal restrictions, and help in regulating traffic in an optimal way. During night time, road markings play important role in road traffic safety and because of that retro-reflective road markings have been developed to insure safety.

One of difficulties confronted by an automobile driver at night time is poor visibility of road side signs and of road markings, variously called road delineators, delineating stripes, pavement

markings and roadway markings. Poor visibility led to the emergence of bright paints or reflective surfaces capable of reflecting the light of the headlights of oncoming vehicles. [4]

Most ceramic materials for different application are synthesized by a conventional solid-state reaction (SSR) method. Fast advancement of the SSR method needed to achieve two situations: "Thermodynamics" and "Kinetics". Based on thermodynamics of defects, in solid state reaction ionic diffusion in an ionic crystal is very sluggish at about room temperature. Therefore, SSR needs a high temperature condition for boosting the reactivity between raw material powders. Due to the high processing temperature, it prompts irregular and uncontrolled particle morphology. On the other hand, liquid phase reactions can arise at relatively low temperatures compared to conventional solid state reactions. However, the final solution product needs additional temperature to dry the solvent and superior equipment for separation.

In this paper, water assisted solid state reaction method (WASSR) at 100°C is employed to synthesize La^{+3}doped $BaTiO_3$ nanoparticles for the application of retro-reflective materials. WASSR is uncomplicated and ceramic materials can be easily synthesized by mixing powdered raw materials with addition of small amount of water. The addition of water as a catalyst will accelerate SSR by providing contact between the starting materials and it was first observed by Toda, K.,et al. in 2007.[5] For example, nano-sized $Ba_{(1-x)}TiO_3$:xEu^{3+}nano-phosphorswere synthesized through this novel and incredibly facile WASSR process at a low temperature of 80 °C and 12 hours.[6]

1.2. **Statement of the Problem**

Modern traffic needs movements of vehicles to be safe under overall circumstances and predominantly at night time in reduced visibility during all seasons and especially in bad weather conditions. Visual guidance in traffic movement is directly related on the visibility and the reflective properties of road side signs and markings.

Safety materials with higher retro-reflectivity provide superior visibility during nighttime.[7] This day's markings, road side signs, safety textile paints and safety helmets are made of retro-reflective materials. Small glass beads are added by dropping on the surface of paint during the process of painting the surfaces in liquid form or by mixing glass beds with the paints during production.

Currently microspheres of glass beads are synthesized via container less flame-spraying, conventional SSR, molten salt methods etc. However, these methods require high temperature (780-1300 ºC) to synthesize high purity glass beads. Such a high temperature process leads to an increase in the processing cost,[5] and needs complicated method and equipment. For example, X. Li et al. successfully synthesized amorphous $La_4Ti_9O_{24}$ microspheres with high-refractive index via container less flame-spraying method .[1]However, flame-spraying is complicated method and high temperature (fed into a C_2H_2-O_2 flame >3000 °C) was used for preparation of the microspheres.

Furthermore, the aforementioned methods might produce larger bead/powder sizes and low densities due to the application of high temperature. Lower bead density gives a low refractive index relative to high density glass beads.[8] In addition, retro-reflecting materials for the application of road side signs, markings, and glass beads with proper refractive index and quality are being imported in Ethiopia.

1.3. Objectives

1.3.1. General objective

The main objective of this current study is synthesis of La^{3+} doped $BaTiO_3$ nanoparticles with high-refractive index using WASSR method which is facile, economical, and unsophisticated method at low temperature.

1.3.2. Specific objectives

The specific objectives of this study are:

- ✓ Synthesis of La^{3+} doped $BaTiO_3$ nanoparticles through WASSR.
- ✓ Investigate phase purity and size of La^{3+} doped $BaTiO_3$.
- ✓ Investigate morphology and structure of La^{3+}doped $BaTiO_3$.
- ✓ Attain the high theoretical refractive index of $BaTiO_3$ via facile WASSR.

1.4. Significance of the Study

In this study, a new and novel material with high refractive index is synthesized which can be used as a retro-reflective material for the application of traffic safety such as in road markings, road side signs, paint for safety helmet, and textile reflective paints. In addition, the cost for producing retro-reflective materials will be reduced due to the application of low production temperature and short production time using uncomplicated and easy method. Furthermore, as a number of road networks in Ethiopia are being designed for high speed traffic, the day to day need for reflecting traffic control materials will increase. Consequently, the development of these materials locally would act as an import substitution and create job opportunities as well as insuring maximum safety conditions. Moreover, the novel material could also be used as external wall paint to regulate internal building temperatures at zero cost of power supply. Since this method can be applied at an industrial and small scale level, the outcome of this study will be also valuable for further industrial scale productions. Finally, this study can be subordinate source of information for researchers on the preparation of other retro-reflective materials.

1.5. Scope of the research.

The scope of this research is limited to synthesis of high refractive index La^{3+}doped $BaTiO_3$.

1.6. Overview of Subsequent Chapters

The remainder of this document is organized into four chapters. Chapter 2 introduces and discusses the literature which forms the foundation for this research effort. It delves into the theories and concepts essential to understanding retro-reflective materials such as pavement marking, road side signs, textile paints, retro-reflectivity, synthesis methods including their producers and some important key researches which have influenced the course of this research. It also highlights some of the key findings and limitations of previous studies. Chapter 3 describes the methodology used to conduct the research. It explains the reasons for using WASSR, experimental procedures, starting materials collection and preparation and characterization. Chapter 4 provides the results for each phase of the research and discussion of the results. Chapter 5 provides limitations of the study, and it concludes with future research opportunities identified during the study.

2. Literature review

2.1. Theories of retro-reflectivity

The course of action to make traffic signs retro-reflective has developed from using reflector button, to using glass beads and then using sign sheeting with micro-cube corners (prismatic sheeting). As sign sheeting has evolved, so have its retro-reflective characteristics.

The advance of retro-reflective materials dates to the 1930's and since this time it has seen some most important growths in improving the efficiency of the sheeting with development in technologies at a microscopic level. The products formed use the glass bead technology that is in use today. Enclosed lens beaded sheeting were developed in the 1940s.[9]Figure 2.1 Show glass bead reflects light back to its source.

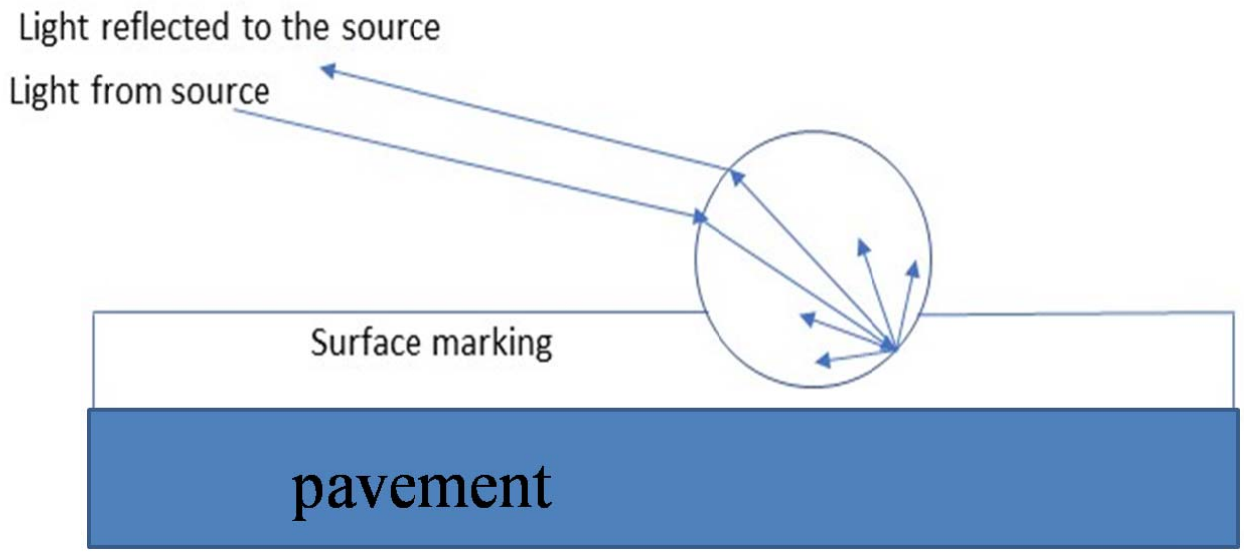

Figure 2.1 How bead reflects light back to its source

The Manual on Uniform Traffic Control Devices (MUTCD) defines retro-reflectivity is a property of a surface that allows a large portion of the light coming from a point source to be returned directly back to a point near its origin.[10] Road markings retro-reflectivity results from vehicle's headlight rays emitted to the road signs. The light ray strikes the surface of road marking, sheeting and signs then return toward the source (to a vehicle).

According to Stephen C. Brich, materials are measured or compared against their coefficient of retro-reflection (RA) at various specified angles and efficient materials have higher RA value. Typically, the higher the RA value, the material appears more easily visible to motorists.[11]

According to AASHTO M247 size of the glass beads is 0.15-0.85μm. Glass beads are tiny spherical glass balls that are used to make pavement marking materials retro-reflective. Glass beads are dropped on top of freshly applied conventional paints and durable materials such as epoxies. In some cases, portions of the beads are mixed in with paint before application (pre-mixed paint).Having a portion of the beads on the surface and in the paint, allow continued retro-reflectivity as the paint wears. The same result can be achieved by using the pre-mixed paints and dropping on beads. The proper application of beads is key in creating the marking's retro-reflectivity.

When a light beam is directed at a glass bead, the majority of the light bounces off but a considerable light beam passes through the glass bead and will refract roughly towards the centre of the rear surface. The light striking the rear surface of the glass bead is internally reflected back through the front surface of the sphere face and again refracted parallel to the direction from which it came. The reflected light diverges in to a cone of rays within three degrees of the source ray instead of in a single direction.[12]

The retro-reflectivity of the pavement marking material makes it visible to drivers at night when their vehicle's headlights reflect off the material. In the case of road markings and signs, light from the headlight of a motor vehicle illuminating a traffic sign and returning that light back to the driver. Paint lines without glass beds will reflect- light randomly in all directions but when round reflective beads are added, light is reflected directly to the source of the light.

The capability of reflecting light back from pavement marking glass beads, road side signs, helmets and safety jackets rest on numerous factors, including the properties of the glass beads themselves. The properties of the beads are controlled throughout the bead manufacturing process and type of retro-reflective materials. These properties can be verified and evaluated preceding to installing a pavement marking to make sure acceptable beads are being used.[13]

Markings support the driver in spotting geometric variations downstream, passing and integration maneuvers and delineate safe travel borders for the driver. These markings play an important role in the driving duty under short, medium and long-range discovery distances. [14]

Materials intended to laser apparatus and protection elements should have high reflectivity and chemical stability at high temperatures. Ceramics have good chemical stability, so far, in most cases, have inferior reflectivities than metals. Therefore, it is essential to advance ceramic materials with enhanced reflectivity. High refractive index materials for optical applications are made principally of Ti-hybrid materials. TiO_2 can be set as nanocrystals in silica matrices or as nanoparticles to integrate directly into a polymer matrix. Silica is the most abundant material and it is major component of glass materials. However, SiO_2-based porous films are the most common type of Antireflective coating[15]as a result this low refractive index matrices were prepared with the base/acid two-step catalytic sol-gel process to adjust refractive index of nanoporous silica films.

Reflection property is dependent on the absorbance rate of materials. The optical absorption edge (Figure 2.2. Shows absorption edge of $BaTiO_3$: xLa at x=0.00) of a material is directly related with the material's band-gap energy and another important factor to be taken into consideration. When using the material for a photonic crystal it determines the wavelength range that the photonic crystal can function.

A photonic crystal cannot be used at wavelengths shorter than its absorption edges obtained. Photonic crystals made of Si, Ge, and GaAs, which have their absorption edge in the near infrared region[15], can be used in the infrared region but cannot be used in the visible. Road traffic safety markings, safety helmets, road side signs and textile safety paints are necessarily to be seen by drivers at night time. Therefore, it is important to synthesize a material which can be used in the visible region.

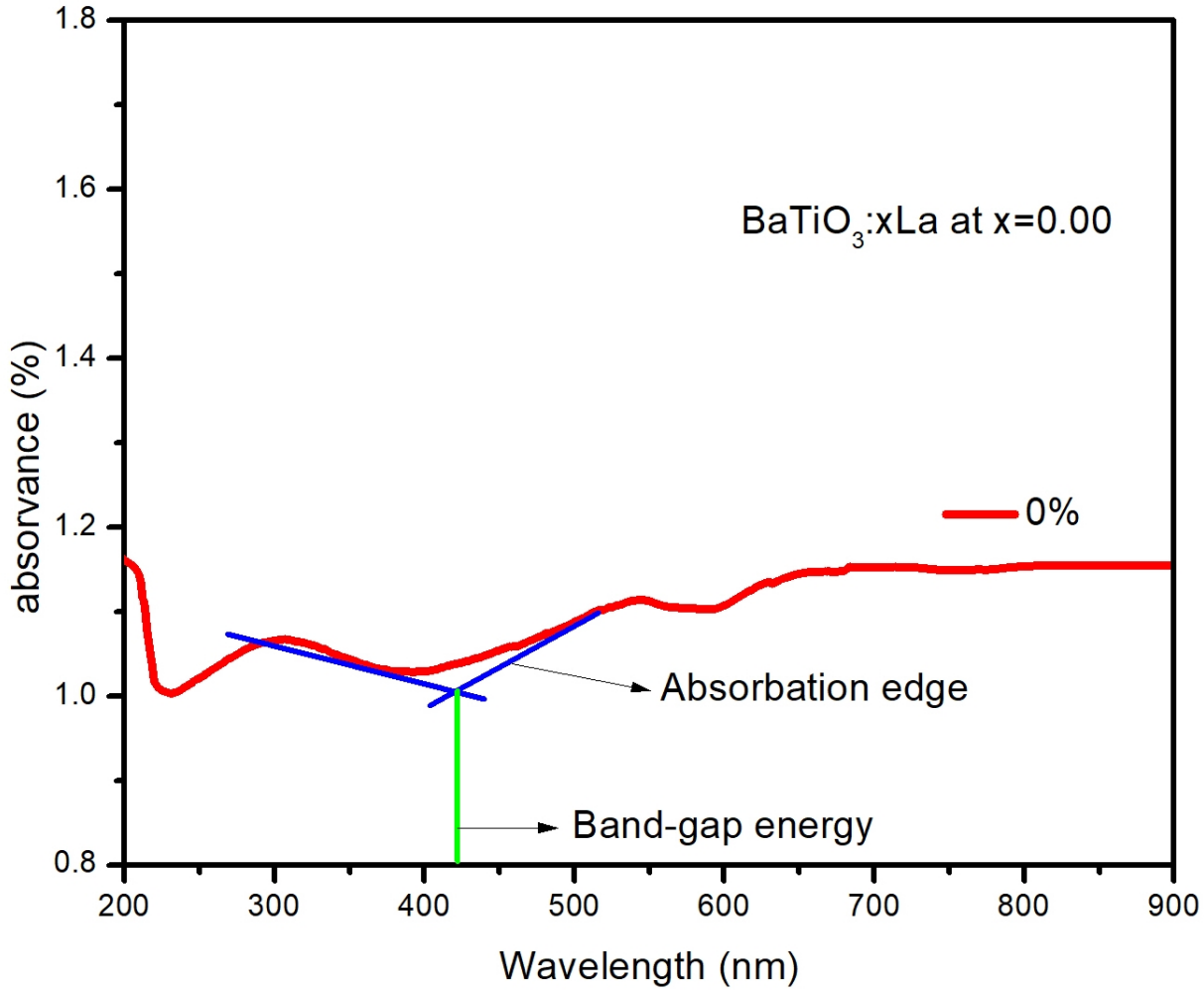

Figure 2.2 Absorption edge of $BaTiO_3$: xLa at x=0.00 (Taken from UV-VIS result).

Ranges of materials from inorganic to organic materials have been used to produce reflective crystals. Dielectric materials are essentially used to compose reflective crystals; however, as the dielectric contrast in a photonic crystal acting a crucial role in the choice of the material to be used is very important. A mixture of titanium oxide and barium peroxide is the fundamental composition of high reflective index glasses contains 60% to 100% by weight.[16] $BaTiO_3$ has fascinated vast attention for decades. It has a perovskite structure, and has decent property which favors the reflectivity.[17] Benefit of retro-reflective materials is that they do not need electrification since they rely on passive (and relatively efficient) reflection of light from source of vehicle headlamps. Subsequently the angle among a driver's sight line to a sign and the light

rays from the driver's headlamps is small, particularly for far viewing distances. As this angle increases, the luminance of a retro-reflective material will generally decrease.[18]

The most usual technique for the application is to place a layer of microscopic glass beads in a translucent polymer layer, followed by coating the composition on top of the protective polymer. On the lower metalized surface glue or epoxy is applied. When using, polyester films have higher mechanical strength, but because of polyester aging (opacification by light) they have less battery life. In the case of acrylic film have a longer life but they have lower mechanical strength during manufacturing signs and manual.[19]

2.2. Properties of $BaTiO_3$

Barium Titanate is white to grey in color when it is in a powder form and a perovskite. It is soluble in acids including hydrofluoric, hydrochloric and sulfuric acids but it is insoluble in water andalkalis.$BaTiO_3$is an electrical insulator when it is in the pure form. On the other hand, while $BaTiO_3$ doped with small metals, nearly all notably yttrium, scandium, samarium, and neodymium and so on it will become semiconducting.

At Curie temperature Barium Titanate undergoes a phase change to cubic from tetrahedral. It also reported single crystals shows negative temperature co-efficient of resistivity. $BaTiO_3$also displays ferroelectric properties and is a great photorefractive material. Table 2.1. shows some property values of $BaTiO_3$.[20]

Table 2.1. Basic property values of $BaTiO_3$

Property	Amount
Melting Point (°C)	1650
Young's Modulus (GPa)	67
Density ($g.cm^{-3}$)	6.02
Hardness (Mohs)	5

2.3. Synthesis of Nanomaterials

For production of materials, there are mainly two approaches, bottom-up and top-down methods. A top-down method starts out with a bulk material, and then utilizes grinding or etching to

achieve the nanosized material. Top-down methods include deferent lithography methods, and are heavily used in the semiconductor processing industry.[21]

Instead of starting with a bulk material, molecules or atoms can be used as starting point for making materials, and these methods are called bottom-up methods. By controlling the assembly of atoms or molecules, materials can be made. For example bottom-up methods include sol-gel and hydrothermal synthesis. Bottom-up methods are often preferred due to easier up-scaling, and for the possibility for being cleaner and more environmentally friendly. Where top-down methods use strong acids or volatile gasses, bottom-up methods could utilize water as reaction media for the correct optimization of the process.

Some of the reported methods for synthesis of Nanophosphors are hydrothermal and sol-gel, which are frequently used to synthesize phosphor and ceramic Nanomaterials. But the drawback of these conventional methods requires superior experimental equipment excluding , strong basic or acidic solutions, or high concentration organic solvents, and washing process to remove the basic or acidic ion or solvents from the surface of particles.[22]La activated $BaTiO_3$ could also be produced using atoms as starting materials on the bottom up production method by WASSR without requirements of further treatments.

2.4. Synthesis of $BaTiO_3$

At room temperature Crystal structure of barium Titanate can be represented by a tetragonal unit cell with size of a_o = 3.992 Å, and c_o = 4.036 Å, but the symmetry turn into cubic above 12O^{o}C., the crystals no longer exhibit ferroelectric properties up on this temperature.[23]

Ceramics are processed from inorganic materials, widely available produced in a maximum tonnage and used by humankind. Until now, there are semi dozen precise ceramic phases and the use of those materials is not only governed in terms of volume, weight, etc., but also in terms of technological significance. For instance, they contain"TiO_2" required high refractive index material in a variety of high volume uses and the key ingredient in electro ceramics. This phases is defined mutually by crystal structure and composition.[24]

Reaction of $TiO_2$and $Ba(OH)_2$to give $BaTiO_3$ under relatively moderate conditions along with in hydrothermal conditions is utmost effective by using very fine, greatly reactive anatase powders.

The obtained product $BaTiO_3$ powders show a high purity and an effective sintering performance consequently densities of around 90% of the theoretical value will achieved.[25]

Humayoun et al. synthesize successfully Eu^{3+}activated $BaTiO_3$ Nano-phosphors through a novel water assisted solid state reaction process by storing the prepared material at a temperature of 80°C for 12 hours. [6] However, it could be prepared by increasing the temperature and reducing the time so that relative cumulative demand of power and the cost of time will become economical. WASSR is an efficient method for synthesis of Nano-sized $BaTiO_3$:Eu^{3+}therefore according to Humayoun et al. observation this method could assist as procedures for the synthesis of other phosphor materials.[6]

Shouhua Feng and RurenXu, also synthesis successfully Tetragonal $BaTiO_3$ in 1999from $Ba(OH)_2$ and TiO_2, free of halide anions, by a hydrothermal method at a temperature of 220°C stored in an oven for several days.[26] However, not only the temperature but also the duration in which the sample to be stored inside oven is high. Then due to the consumption of power and time the synthesis method is not economical.

X. Li et al. synthesize successfully amorphous $La_4Ti_9O_{24}$ microspheres with high-refractive index via container less flame-spraying method in 2017 and prepared a material with greatly increased reflection of glass slide as substrate in the range of 300–2000 nm, which was valuable for protective reflective helmet or clothes, road side signs.[1]It can be also used as heat reflective layer, which can sort out the urban heat island effect surfaces that need illumination from reflection of light rays.

According to X. Li et al. ,the mixture of starting material was spray dried through the feed rate set as 10 mL/min, inlet and outlet temperatures were maintained at 190 °C and 120 °C, correspondingly.[1]In addition, spray-dried powders were oven dried and then fed into a C_2H_2-O_2 flame (>3000 °C). Furthermore, The oven dried prepared material was washed with water and then thermally heated at 500 °C for 12 hours therefore Complexity of preparation method followed by high application of temperature makes the product uneconomical and needs complicated equipment which makes the preparation difficult comparing to water assisted solid state reaction. Therefore, it is important to study each synthesis methods and choose simple,

economical and efficient synthesis method. On current work some of the widely used synthesis methods are discussed briefly as follows.

2.4.1. Synthesis of $BaTiO_3$ using Hydrothermal

Hydrothermal synthesis is widely used for synthesis of nanomaterials, and especially nanoparticles because of its flexibility and good crystallinity in the final products. A common definition for hydrothermal synthesis is a chemical reaction carried out in an aqueous media at elevated temperature andpressure.[27]Ifthereactionmediaisanorganicsolventinsteadofwater, it is called solvothermal synthesis. Both hydrothermal and solvothermal synthesis are carried out by heating the precursors, or chemicals, in a closed vessel called an autoclave. Increased temperature and pressure leads to an increase in solubility and reactivity of the chemicals. However, the drawback of increased in temperature is related to the cost of production and the produced product will have large particle sizes for instance.

Zhu et.al Characterize successfully Barium Titanate$BaTiO_3$ Powder produced by hydrothermal method at 220°C. Barium hydroxide octahydrate and anatase were used as starting materials and KOH as a mineralizer and characterization was done using XRD, SAED, Raman spectrum, SEM, TEM, and HR-TEM. From the XRD result it was observed that the $BaTiO_3$nanopowders was in cubic phase, while the tetragonal phase $BaTiO_3$ detected from Raman spectra of the prepared nanopowders in which point to that the $BaTiO_3$ nanocrystals with some tetragonallity and it was metastable cubic phase. [28]

In addition according to Raman spectroscopy experimental result, he discovered a distinctive spectrum to the nanoparticles having broader peaks compared to$BaTiO_3$ single crystals, which is due to the arbitrary allocation in the powder. He concluded that the experimental peaks located near 178, 521, and 710 cm^{-1}arethe tetragonal $BaTiO_3$ phase. And also, the peaks about 148, 400, and 645 cm^{-1} comes from the consequence of unreactedTiO_2 as a result the Raman spectrum of anatase TiO_2 is dominated by a large peak at about 150 cm^{-1}. According to Zhu et.al on XRD result the diminutive amounts of un reacted anatase are not easy to identify however they can be detected in Raman spectra. Therefore, when we compare this method with water assisted solid state reaction (WASSR) the cost is high due to the demand of high temperature and extended

heating time which is 220^{o}c for 3 days in an oven. While, in the case of water assisted solid state reaction (WASSR) it can prepare at 100^{o}c and below with in shorter heating time which is more economical. In addition while reaction process by hydrothermal method at 220°C takes place it is observed that the availability of unreacted TiO_2(anatase) . Therefore, the reaction is not complete. As a result it is important to look another synthesis method which is economical and can produce complete reaction to have pure result of $BaTiO_3$.

2.4.2. **Synthesis of $BaTiO_3$ using Sol-gel**

Sol–gel is a process of preparation of ceramic materials that includes the preparation of a sol, gelation of the sol, and removal of the liquid from the prepared material. The gel holds liquid existing in fine interconnected channels, and it needs to dry before it converts to a valuable material. However, the capillary pressure will increase during drying by evaporation under normal conditions accompanied by shrinkage of the gel network. The resulting dried gel is called a zerogel. The capillary pressure is large in polymeric gels due to the pores are normally much finer relatively tin colloidal gels; thus, problems can be come upon with warping and cracking of the gel.[29] Two broad approaches used to avoid these difficulties. The use of chemicals added to starting materials solution before gelation, which is called drying control chemical additives (DCCAs), allow relatively fast drying. The gel undergoes relatively little shrinkage. The dried gel (aerogel), is therefore fragile and may shrink considerably during firing.[29] during this synthesis method we can observe that high level of temperature is important and the process is complicated needs Solution stirring, gel and solvents separation, gel draying calcinations and soon. As shown on table 2.2 synthesis of $BaTiO_3$using Sol-gel method needs firing temperature of 500- 1300 ºc but WASSR is easy process which is simply mixing starting materials using mortar and pistil and stored at a temperature of bellow 100ºc to synthesis $BaTiO_3$. As a result WASSR is relatively easy and uncomplicated. Some of results from sol-gel synthesis are discussed on table 2.2.

Table 2.2. Previous researches based on sol-gel synthesis of $BaTiO_3$

Precursors	Product	Temperature	Time(maximum)	Ref.
$Ba(acac)_2.2H_2O$, $Ti(OPri)_4$	$BaTiO_3$	-solution stir&refluxing-80◦C -gel & solvents separation-80◦C - gel draying- 100◦C - gel powdercalcinations-1000◦C	For all process 15h	[30]
$Ba(CH_3COO)_2$, Y_2O_3&TiO_2	$BaTiO_3$, Ba_2TiO_4	-stirred at 60–90 ◦C. - dryingat 90 ◦C - gel powdercalcinations-900◦C - sintered at 1300 ◦C	For all process 34h	[31]
Barium acetate & titanium bis dihydroxide	$BaTiO_3$	- solution stir&refluxing-100◦C - drying at 80◦C - pyrolyzed at 300◦C -heated at 800◦C -firing500 to 1100◦C	For all process 15 h	[32]

M.Cernea et.al. Use Titanium isopropoxide and barium acetylacetonate as a starting material and he synthesize$BaTiO_3$ powder by sol-gel method successfully. [30] However, the process is done at high temperature. During refluxing the mixture solutions of starting materials used a temperature which is around 80 °C, for separating the gel and removing the solvents 80°C, drying the gel used temperature was 100 °C finally for calcinations of the gel powders was used 1000 °C. Not only consumption of high temperature it needs extended time for different processing stages for example for adding glacial acetic acid 2 hours, to stir the mixture 8 hours and then 3hours to dry the gel.

B. Lee, J.Z.et.al in 2001 successfully characterize $BaTiO_3$ [32] on short time but higher temperature than M. Cernea et.al, However, relatively to Kareiva, A.et.al he synthsize at low temprature and time.

Kareiva, A.et.al. Sucssesfully synthsiz $BaTiO_3$ via- sol-gel method. [31] He used starting materials and range of temprature as indicated on table.2.2. However, the temprature and time is relatively higher than the range imployed by M. Cernea.et.al and B. Lee, J.Z.

Therefore, from the different researches listed above and discussion we can observe that the sol-gel method is complicated and it takes long period in addition to high temperature. Therefore, the synthesis method is uneconomical relatively to WASSR method.

2.4.3. **Synthesis of $BaTiO_3$ using Solid state Reaction**

A powder system in solid state reaction depends on a number of parameters. Consist of the reactant chemicals nature and the as prepared material; size and its distribution; and particle shape; the comparative sizes of the precursor particles in the combination; the regularity of mixing, atmosphere in which the reaction takes place; temperature; and duration of reaction.

The reaction speed will decline with a raise in particle size of the starting materials for the reason that, on average, the diffusion distances will rise and the reaction speed will rise with temperature. Usually, the homogeneity of combination is one of the most parameters.

Synthesis of powder using solid-state reactions (SSR) quality is also an essential concern for advanced ceramics. The powders are usually agglomerated and a grinding is almost for all time required to synthesis powders with enhanced characteristics. Grinding in ball mills affects the product purity during grinding contamination of the powder with impurities will be seen.[29]Unfinished reactions, mainly in inadequately mixed powders, could produce unattractive phases. Moreover, shape of the particle of ground powders is generally difficult to control on solid state reaction.

Simon-Seveyrat, L.et.al using precursor of $BaCO_3$ and TiO_2he synthesized $BaTiO_3$ successfully. [33] And from the characterization result observed that $BaTiO_3$is perovskite phase and happening to emerge at temperatures among 780 and 880 ^oC in addition to that at 1050^oC $BaCO_3$ were not seen except a slight amount of rhombohedral $BaCO_3$ but $BaTiO_3$ is perfectly produced. However, it is also observed that $BaTiO_3$proceeds by the development of predominantly Ba_2TiO_4phase. It is detected as extremely little amount in the mix, at peak 2θ =28 between 880 and 1050 ^OC.

2.5. Water assisted solid state reaction (WASSR)

Conventional Solid-state reaction (SSR) method is slow at around room temperature and requires a high temperature for increasing the reaction process among starting powder material. High temperature processing leads for the result of irregular and uncontrolled particle morphology.[5]While some liquid phase reactions can occur at comparatively low temperatures than the conventional solid state reactions, solution process requires to dry the solvent and to use special equipment for the separations.

After Toda, K., et al. showed the advantages of this method as compared to other conventional methods it was demonstrated that, WASSR method is a novel synthesis method for achieving fine ceramic nanomaterials at low temperatures less than 100 ºC starved of thermal and physical post-treatment. WASSR method is likewise did not involve a chemical treatment using basic or acid solution or organic solvents all through synthesis processing.[34]

The quantity of dissolved starting materials in water is insignificant during the WASSR method. This implies that the process is also different from several conventional solution reactions, which arises by the dissolution of the starting materials. Furthermore, the WASSR method takes place without strong applied mechanical load just simple hand mixing or storing. Consequently, the working mechanism of WASSR synthesis method is unlike to the conventional solid state reaction, solution reaction. A solid acid-base reaction is a likely mechanism.

2.6. Previous Studies via WASSR

Over the past recent years, numerous researches have been conducted on ceramic materials and Nanoparticle phosphor materials. Many of the researches where successfully synthesized phosphor materials and there is a considerable variety between both the variables considered for the synthesis but the same preparation approaches. This section discusses the key researches listed in Table 2.3. which have influenced the course of this research.

Table 2.3. List of materials synthesized by WASSR

Starting materials	Amount of water	Stored duration of time	Result	Reference
$Mg(OH)_2$ and V_2O_5	10%	24 h at 353K	$MgV_2O_6.2H_2O$	[22]
Rb_2CO_3 and V_2O_5	10%	6h at 353K	$Rb_3V_5O_{14}$	[35]
Y_2O_3 and V_2O_5	10%	24 h at 353K	YVO_4	[36]
$SrCO_3$ and MoO_3	10%	12 h at 313K	$SrMoO_4$	[37]
Y_2O_3, V_2O_5 and Eu_2O_3	10%	3 h at 297 K	YVO_4: Eu	[38]
$LiOH.H_2O$ and SiO_2	10%	10-180min at 353K	Li_2SiO_3	[39]
Na_2CO_3, EU_2O_3, GdO_3 and MoO_3	10%	48 h at 353 K	$NaEU_{1-x}Gdx(MoO_4)_2$	[40]

Kim SW, et al. A yellow $MgV_2O_6{\cdot}2H_2O$ nanophosphor was synthesized by Kim Sw, et al., 2017 through WASSR method. [22]During material preparation he added 10% of water as a catalyst at 353 k heated for 24 hours. Kim SW., observe parameters from XRD data of the $MgV_2O_6{\cdot}2H_2O$ nanophosphor was orthorhombic structure; with a lattice parameters of a = 0.5551 nm, b = 1.0753nm, c = 1.1841 nm, and V = 0.7069 nm^3. From the result in which he obtain MgV2O6·$2H_2O$ was a layered structure containsMgO_6 octahedral and VO_4 tetrahedra on b axis. He observed a wide optical absorption band in the near-UV region because of charge-transfer transition from the O^{2-} 2p orbital to the V^{5+} 3dorbital in the $[VO_4]^{3-}$ group, and it showed a wide-ranging peak related to the emission of yellow light at 562 nm. His research was novel and précis crystallographic structure data was obtained and it is observed that the optical property of $MgV_2O_6{\cdot}2H_2O$ is phosphor.

Kenji Toda, et al., 2017 [41]synthesize successfully a Nano $SrMoO_4$by WASSR method at room temperature. In addition, he successfully synthesized several ceramic materials, like YVO_4:Eu^{3+},

$BaTiO_3$, $LaPO_4:Ce^{3+},Tb^{3+}$, and $NaEuMo_2O_8$ at low temperature (313 K). [41]The work also summarized and proposed WASSR is low cost and low temperature synthesis technique, According Kenji Toda his proposal has shown a potential for an industrial application for ceramic materials synthesis processing. But application of the method is not yet applied at any industrial productions.

The purpose of his effort was to show that the method is very simple and can synthesize many ceramic materials just by storing or mixing raw materials added a small amount of water in a reactor at low temperature below 373K . He also discussed that as spherical morphology of the WASSR method sample is resulted from rapid ionic diffusion during the reaction and "the reaction mechanism of WASSR synthesis methods is different from the conventional solid state reaction, mechano-chemical reaction and solution reaction"[37]but he was not able to identify understandable mechanism. He guesses the possible mechanism is new type water accelerated solid acid-base reaction on the surface .So that the water covers the surface of the starting material powders. As a result the solid acidity and solid basicity of the powder starting material promotes the solid acid-base reaction of starting materials at the contact surface of the particles.

2.7. **Techniques to Study Nanoparticles**

Nanoscale materials frequently provide diverse properties than their bulk counterparts, The properties of nanoscale materials reactivity at molecular level include electronic, optical and chemical increase because of their high surface-to-volume ratio.[42]The multi and cross-disciplinary character of Nanoscience is reflected in a number of techniques that are essential to solve and know the properties of nanomaterials. Given the extent of the subject, it is provided below only a brief overview of the essential techniques to study nanoparticles (NPs).

2.7.1. **Crystal structure Size and Shape**

The primary questions frequently asked about Nanoparticles are worried with the state of aggregation, size, and morphology; straight imagining of particles by scanning or transmission electron microscopy (SEM and TEM, respectively) is a model instrument for answering such questions. In SEM and TEM a beam of high-energy electrons is applied towards the sample, and signals follow-on from electron-sample interaction are analyzed.[43]Transmission Electron Microscopy (TEM) and High-Resolution TEM (HRTEM) are vital tools for the characterization

of size and shape of NPs. HRTEM may also produce information about the crystal structure and chemical composition of single NPs when linked to electron diffraction analysis and energy-dispersive X-ray spectroscopy (EDS),[44] respectively. Electron microscopy techniques are advanced from powerful magnifying tools that offer images to enormously multipurpose measurement devices that offer structural, chemical, electronic, or magnetic information down to the atomic scale. X-Ray diffraction (XRD) can be used to define crystal structure of nanomaterials and may also produce information about the NP size.

2.7.2. **Optical spectroscopy**

Diverse materials including nanomaterials optical properties are identified using Optical spectroscopic methods. The techniques are generally related on measuring absorption, scattering or emission of light that contains related data about properties of the materials.[45]

A combination of spectroscopic technique is needed to know the optical properties and electronic structure of NPs. Absorption, photoluminescence (PL), and PL excitation (PLE) spectroscopy offer information about the energy level structure. This technique provides complementary information regarding the fast relaxation of electrons and holes.

Common theme throughout most of the synthesis technique discussed on the literature is application of high temperature, long period time for the process and some of the products are convoyed by littlie secondary impurities. Therefore, due to the application of high power consumption and longer time, most of the methods are not economical compared to WASSR. Thus, WASSR is economical and uncomplicated method to synthesize $BaTiO_3$ nanoparticles and can be implemented by using low and cheep heating temperature which is less than or equals to 373K at short period of time. However, the characterization method is similar. In addition, the method is promising for industrial applications. The aforementioned researches on WASSR method has shown that the size and morphology of the product in water assisted method is affected by the amount of added water and heating time. However, there is no literature or study related to retro-reflective materials production using WASSR method and all researches focus on synthesis of phosphors using WASSR than retro-reflective material.

3. Materials and Method

3.1. Materials

The starting materials are reagent grade, Titanium Oxide Nanoparticles (TiO_2) Anatase, 99.9%, 5 nm. And Lanthanum Oxide powder (La_2O_3), 99.9% from SkySpring Nanomaterials, Inc, Texas, U.S.A. Hydrated Barium Hydroxide Ba $(OH)_2.8H_2O$, 98%,deionized water and ethanol 99.9% was collected from local market(Addis Ababa). For the preparation of La doped $BaTiO_3$with the empirical formula $Ba_{(x-1)}$ LaxTiO3 were used.

3.2. Experimental

The $Ba_{(1-x)}TiO_3$: x La was prepared by water assisted solid-state reaction method. The starting materials was weighed according to the stoichiometric ratio $Ba_{(1-x)}TiO_3$: xLa, where x= 0.00 ,0.01,0.5 and 0.10for a final product of 2gm after experimental trials. Then weighed precursors were carefully homogenized by grinding the mixture dray and then mixed with the addition of 8% deionized water (160ml) as a reactor using a mortar and pistil for 15 minutes for the final product.

According to the target designed product composition of the new synthesized oxide the amount of starting material used $Ba_{(x-1)}xLaTiO_3$ for x=0.00,0.01,0.05 and 0.10 are shown in Table 3.1.

Table 3.1. Weight of starting materials according to stoichiometric ratio.

Targeted designed product	Starting material	Weight(g)
$BaTiO_3$	$Ba(OH)_2.8H_2O$	2.7044
	TiO_2	0.6850
$Ba_{(x-1)}xLaTiO_3$, at x =0.01	$Ba(OH)_2.8H_2O$	2.6772
	TiO_2	0.6550
	La_2O_3	0.0308
$Ba_{(x-1)}xLaTiO_3$, at x =0.05	$Ba(OH)_2.8H_2O$	2.5690
	TiO_2	0.6850
	La_2O_3	0.1542
$Ba_{(x-1)}xLaTiO_3$, at x =0.10	$Ba(OH)_2.8H_2O$	2.4323
	TiO_2	0.6850
	La_2O_3	0.3086

After mixing the starting materials, the finely ground powders were filled in to caped bottle and transferred inside automatic oven at low temperature which is adjusted to 373 K for six hours. Different experiments were carried out, for keeping time of seventy two hours, twelve hours and six hours, and all the keeping times produced the desired product, $Ba_{(1-x)}TiO_2$: x La. Thus, the shorter keeping time inside the oven, six hour, was selected being economical. After completion of six hours keeping time, the sample was removed from the oven and ground using mortar and heated inside the oven at 373 K for one hour to remove the remaining water inside the prepared sample. Figure 3.2 shows the Schematic representation of WASSR synthesis procedure of the preparation of Nanoparticles of $Ba_{(1-x)}TiO_2$: x La.

WASSR Preparation procedure

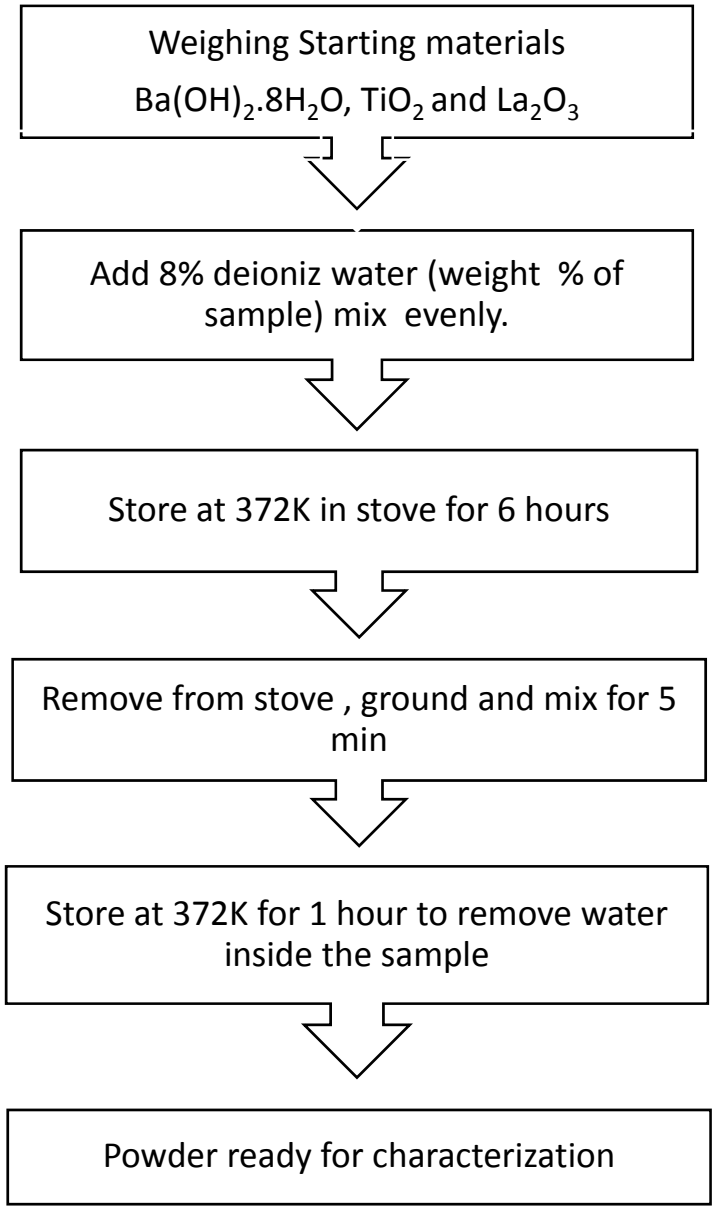

Figure 3.1 Schematic representation of WASSR procedure for preparation of $Ba_{(1-x)}$ TiO_3: x La.

4. Characterization

X-ray is a type of electromagnetic radiation and has greatly shorter wavelengths including significantly higher energy relative to visible light. In diverse ways X-rays can be created. However, the technique nearly all used in x-ray diffraction experiments is to have accelerated electrons hit a target anode, as a result a wavelength characteristic of the anode material will emit. [46]

X-ray diffraction (XRD) is a non-destructive analytical technique based on Bragg's Law, which provides information about the chemical composition and crystallographic structure of materials. In this work, using X-ray diffraction (XRD) pattern phase of $Ba_{(1-x)}$ La_xTiO_3particles were obtained with an X-ray diffractometer (Shimadzu XRD-7000S)using Cu Kα radiation. All data were measured in λ=0.15406 nm,40ku,30mA, step size of 0.02° (2Ɵ) , scan speed at 3°/min and scan range from 10° to 80°.

Samples were mounted on zero background substrates then X-ray diffraction pattern collection was done. In addition, powder samples were mounted just sprinkled on as a fine powder and were smooth flat surface for diffraction to be taken from. To confirm the structure of the as prepared material the spectra of Raman frequency were recorded at a range of 50 cm^{-1} to 850 cm^{-1}.

The prepared material Morphology and the chemical composition of the new material $Ba_{(1-x)}La_xTiO_3$were observed by scanning electron microscopy (SEM) and energy-dispersive spectroscope (EDX)operated at 10kv was perform and to prevent shifts in the picture caused by charging effects, the sample was coated with a thin gold layer (Agar Sputter Coater). a thin layer was sputtered onto the samples prior to imaging. Photographs of the samples also acquired using a digital compact camera.

UV–Vis-NIR spectrophotometer was employed in characterization optical retro-reflection spectra. The cone angle of collection was 1° which is within the range of most commonly used for traffic control devices. The spectra were recorded over a wavelength range of 200 to 900 nm.

5. Results and discussion

a. X-ray Diffraction and Phase Identification

In this work data collected for the profiles of as prepared new material $Ba_{(1-x)}xLaTiO_3$ is shown in confirmation with the International Center for Diffraction Data (ICDD)database and discovered similar hkl reflection positions as given for $BaTiO_3$ on ICDD 00-31-0174.The strongest three peak reflection of the as prepared material and the standard data base for $BaTiO_3$ is located at nearly the same positions at 2θ =31.2959, 55.7077 and 44.8447, but as shown on Fig.5.1. a clear inconsistency is obvious in terms of additional smaller diffraction reflections on the prepared material.

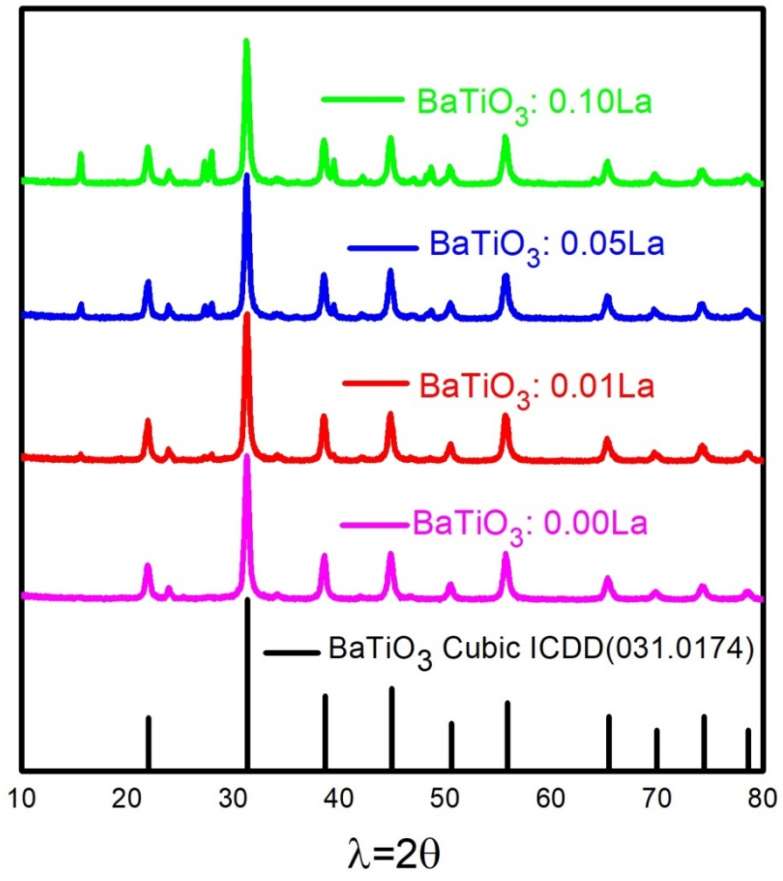

Figure 5.1 XRD pattern for $Ba_{(1-x)}TiO_3$: x La

Characteristic is expressed on the pattern of powder diffraction for a substance, it is like a fingerprint and measured diffraction pattern is somewhat likely to be reproduced by the specimen of uncontaminated substances. If Specimens having two components or more. In the Hanawalt method, each substance is characterized by the d-values of the three strongest diffraction peaks.[47]

The d_1, d_2,and d_3 values for the three strongest diffraction peaks of the as prepared material (at 2θ =31.2959, 55.7077 and 44.8447) together with the relative intensities (I/I_1) are used to investigate the corresponding pattern in the database. Analysis is done fitting the exact match between the diffraction data of x-ray and those of the standard database result for ICDD 00-031-0174. According to the result obtained from the experimental data good agreement with the standard data sheet were observed.Table.5.1 shows comparison related to the d values.

Table 5.1. Comparison of d-spacing and I/I_1 for three strongest diffraction peaks using the result found from x-ray diffraction and ICDD 00-031-0174.

Parameters	Value for x-ray diffraction for as prepared material	Value for ICDD 00-031-0174 From the standard data base
d_1	2.85586	2.85000
d_2	1.64870	1.64450
d_3	2.01950	2.01600
I/I_1 at d_1	100	100
I/I_1 at d_2	32	25
I/I_1 at d_3	32	35

However, the automatic search by computer was employed instead of manual searching together with the automatic calculation of d values as output of an automatic diffractometer.

The XRD diffraction results for the powder indicate formation of tetragonal phase of $BaTiO_3$. The appearance of X-ray reflections at 2θ = 30.4228, 31.2959, 38.5628, 44.8447, 50.4655, 65.2994, 69.7979, 74.2311 and 78.4939is in correlation with ICDD (00-31-0174) standards. According to literature[48], the structure of BaTiO3 may be cubic at room temperature. From the x-ray result distinguishing tetragonal and cubic phases is challenging because the result for both patterns of cubic and tetragonal phases are similar. The major dissimilarity is that the peak for the cubic phase is single while for the tetragonal phase will split in to two at 2θ = 45°[49]as shown on Fig.5.2.

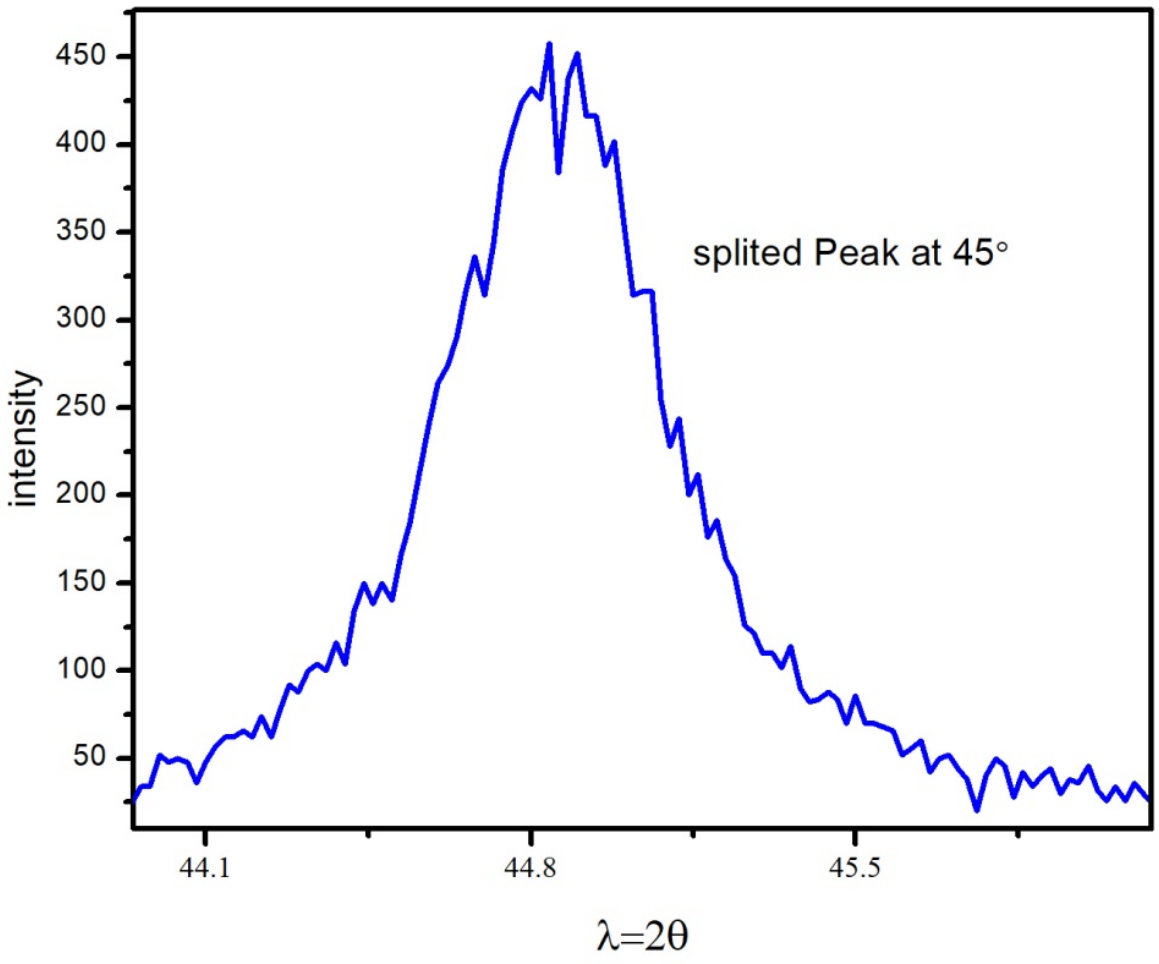

Figure 5. 1. X-ray peak result at2θ = 45°

As shown on Figure.5.2.it is observed that the as prepared material is in a tetragonal phase. In this work, finding such splitting was done but it was not easy due to the polycrystalline environment of the broadened peak width. However, this could be confirmed using the Raman spectroscopy.

The XRD patterns of the as prepared $Ba_{(1-x)}xLaTiO_3$at x=0, x = 0.01,x = 0.05 and x = 0.10 including XRD pattern for standard database ICDD 00-031-0174is shown on the profile pattern (Fig.5.1.) all peaks from the standard database of $BaTiO_3$ are indexed at (100), (110), (111), (200), (210), (211) , (220) , (300), (310) and (311) and the indexes are well match with result of as prepared $Ba_{(1-x)}xLaTiO_3$: values. Using the obtained peak values Calculations executed to yield information about the sample such as phase composition by comparison to a database of reference patterns, Unit cell lattice parameters calculated from peak positions, Crystal system. Determined by indexing observed peaks and systematic absences, Crystallite size calculated from peak widths and/or shapes, A number of engineering indexes are also calculated from peak list information.

From the result of XRD pattern peaks we can observe that the sample at x = 0.05 and at x = 0.10 there is mismatch with standard database ICDD 00-031-0174 values at peak where $2\boldsymbol{\theta}$ =15.6668 and15.6684 respectively the standard database do not include this peaks in addition smaller diffraction reflections for impurities are also appeared.

According to the result obtained from XRD test data and fitted to the database this smaller peaks ($2\boldsymbol{\theta}$ =15.6668 and15.6684) stands for $Ba_2La_2O_5$. Therefore, we can conclude that La is not fully substituted in a place of Ba at x=0.05 and 0.10. On the other hand when x=.01 the pattern where observed matched with ICDD values (00-031-0174) without appearance of significant additional major peaks.

X-ray diffraction analysis is not only to classify the phase of unidentified substance, as well as the guess of the lattice parameters, but as well to find out the concentration of the phase in the mixture. The x-ray diffraction peak profile is also engaged to guess the particle size of very small crystals called “crystallites” in a powder specimen.[47] X-ray Diffraction peak positions can be used to calculate unit cell dimensions. The unit cell dimensions can be correlated to interatomic distances. Interatomic distances can change due to, temperature; sub situational doping and stress

will be reflected by a change in peak positions. The diffraction peak width contains micro-structural information while applying full width of half maximum (FWHM) values from the X-Ray Basic data for the prepared material and it is found that the crystallite size and average crystallites size of $Ba_{(1-x)}TiO_3$:xLacan be calculated from XRD pattern data using Scherrer's formula, which is

$$Particle\ Size\ (D) = \frac{k\lambda}{d\cos\theta} \qquad \ldots\ldots\ldots\ldots\ldots\ldots\ldots\ldots\ldots \text{eq. (5.1)}$$

Where λ=0.15406 nm (Wavelength of the x-ray sources),

d is the full width of half maximum (FWHM) of a diffraction peak can be read from sample x-ray diffraction characterization result (radians),

θ is the diffraction angle at peak position (radians) ,

K = 0.89 (Scherrer constant) and D is Crystallites size (nm).

During Calculations it is important to determine peak positions and FWHM result data from XRD pattern and using the Scherre equation for the calculation of crystallites size. Therefore for Particle size (D) of the as prepared $Ba_{(1-x)}TiO_3$:xLa at all proportions ratios (value of x) when we substitute the determined data from XRD in the equation the result was found to be as shown bellow on Table.5.2.

Table 5.2. Average particle size (nm)at x=0.00,0.01,.05,and 0.10.

Value of x for $Ba_{(1-x)}TiO_3$:xLa	Average particle size (nm)
0.00	19.74
0.01	19.39
0.05	19.40
0.10	21.64

Therefore the crystal size is ranging from 19.39 to 21.64 nm and it is observed that the amount of doping of La affect the crystal size as the amount of La increase the crystal size also increasing. Moreover, the impurity of the as prepared material also rises. Nanocrystallite size materials produce peak broadening that can be quantified but once the crystallite size is larger than a maximum limit, the peak broadening cannot be quantified. This creates an upper limit to the crystallite size that can be calculated.

We can observe that from the specimen X-ray diffraction profile result when broadening is large the specimen will be highly nanocrystalline . To study the relationship in between the broadening and the crystallite size observing the calculated crystal size and FWHM data is important and it is shown on Table.5.3.And we can observe that while the FWHM value increase the specimen size will decreases and will become highly nanocrystaline on the other hand when FWHM value decrease the specimen size will be increased.

Table 5.3.Compartion of calculated crystal size with FWHM for Ba(1-x)xLa TiO_3 at x=0.00

Peak position 2θ (°)	FWHM D_{size}(°)	Dp (nm)
21.9827	0.4976	16.26
23.9656	0.3950	20.56
30.4228	0.2934	28.06
31.2959	0.4949	16.67
32.2806	0.3866	21.39
38.5628	0.5072	16.59
44.1912	0.2800	30.62
44.8447	0.5296	16.23
45.5304	0.2800	30.77
50.4655	0.5150	17.05
55.7077	0.5564	16.15
65.2994	0.5823	16.20
69.7979	0.5533	17.51
74.2311	0.6820	14.61
78.4939	0.5900	17.39

In addition to the degree of nanocrystallite size, Non-uniform lattice strain and defects will also cause peak broadening careful evaluation is required to separate all of the different potential causes of peak broadening.

Indexing of powder patterns in tetragonal crystal becomes difficult because number of unknown parameters to be determine increases. On cubic crystal we have only one unknown parameter, that is the cell edge a, while on non cubic crystals there are two or more, due to this in order to index the patterns of tetragonal crystals formulas will be used[50]

The primary step in identifying crystal structure of a polycrystalline specimen is listing the diffraction pattern over as wide range of 2θ, usually with diffractometry. Make sure Sample preparation ensures arbitrary orientation of the individual particles of powder, to have any meaning in terms of crystal structure the experiential relative intensities of the diffraction lines. Following obtaining of the pattern value of $\sin^2\theta$ is calculated for each diffraction line; this result of $\sin^2\theta$ value is the inputs to resolve the cell size and shape. Or we can calculate d value of each line and work from this set of numbers.

The analysis of peak positions between both profiles is nearly identical which means Lanthanum replaced Barium sites successfully specially at x=0.01 Barium site is replaced with Lanthanum without impurities.

b. Scanning Electron Microscopy (SEM):

Figure 5.3 to Figure 5.6 show the SEM micrograph, EDS mapping and Elemental analyses of the prepared $Ba_{(1-x)}$ TiO_3: x La at x= 0.00,0.01, 0.05 and 0.10, respectively.

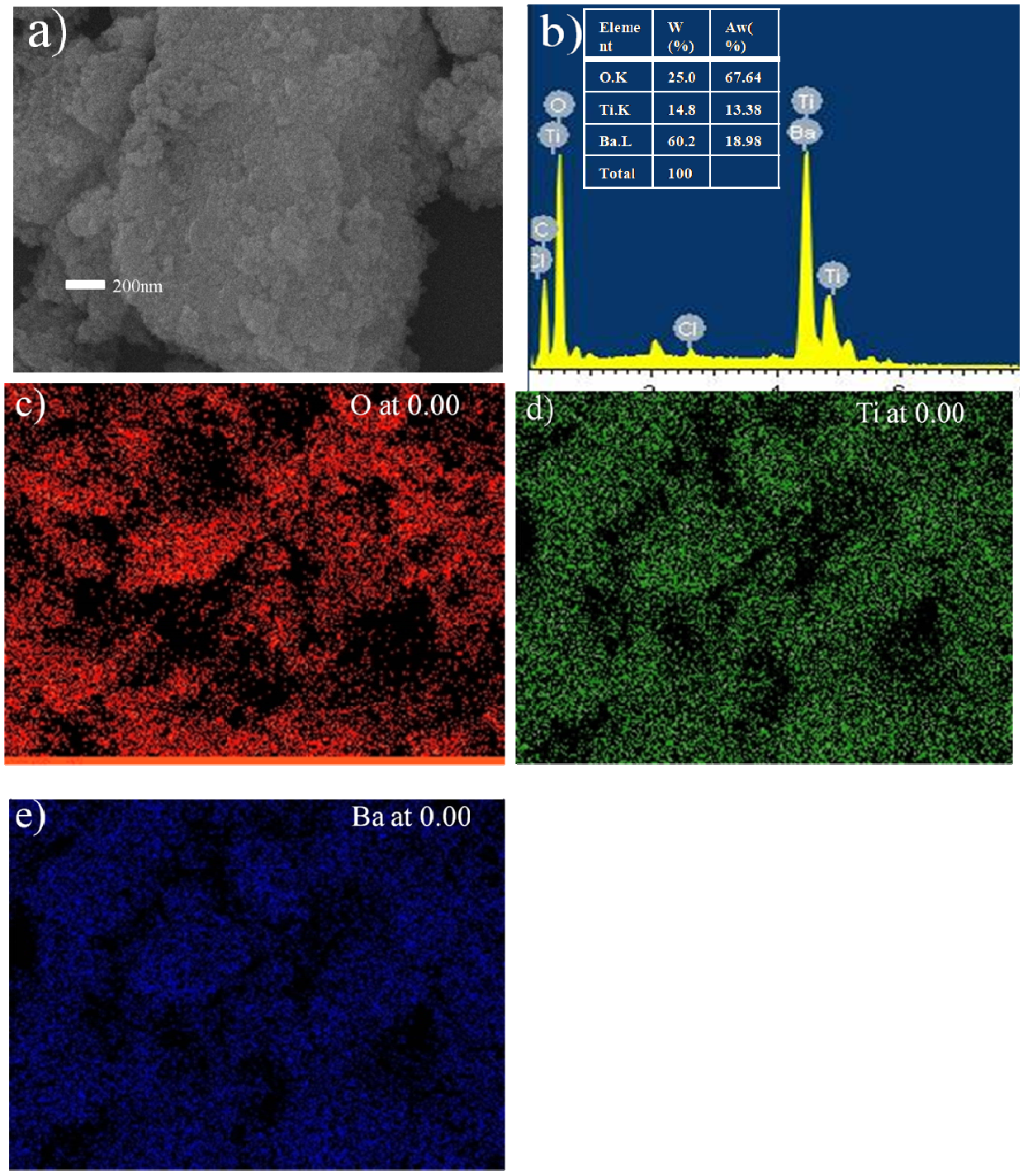

Figure 5. 2Result of $Ba_{(1-x)}TiO_3$: x La at x=0.00 (a) SEM images, (b) EDS result(c) (d) and (e) EDS mapping image of O,Ti and Ba respectively

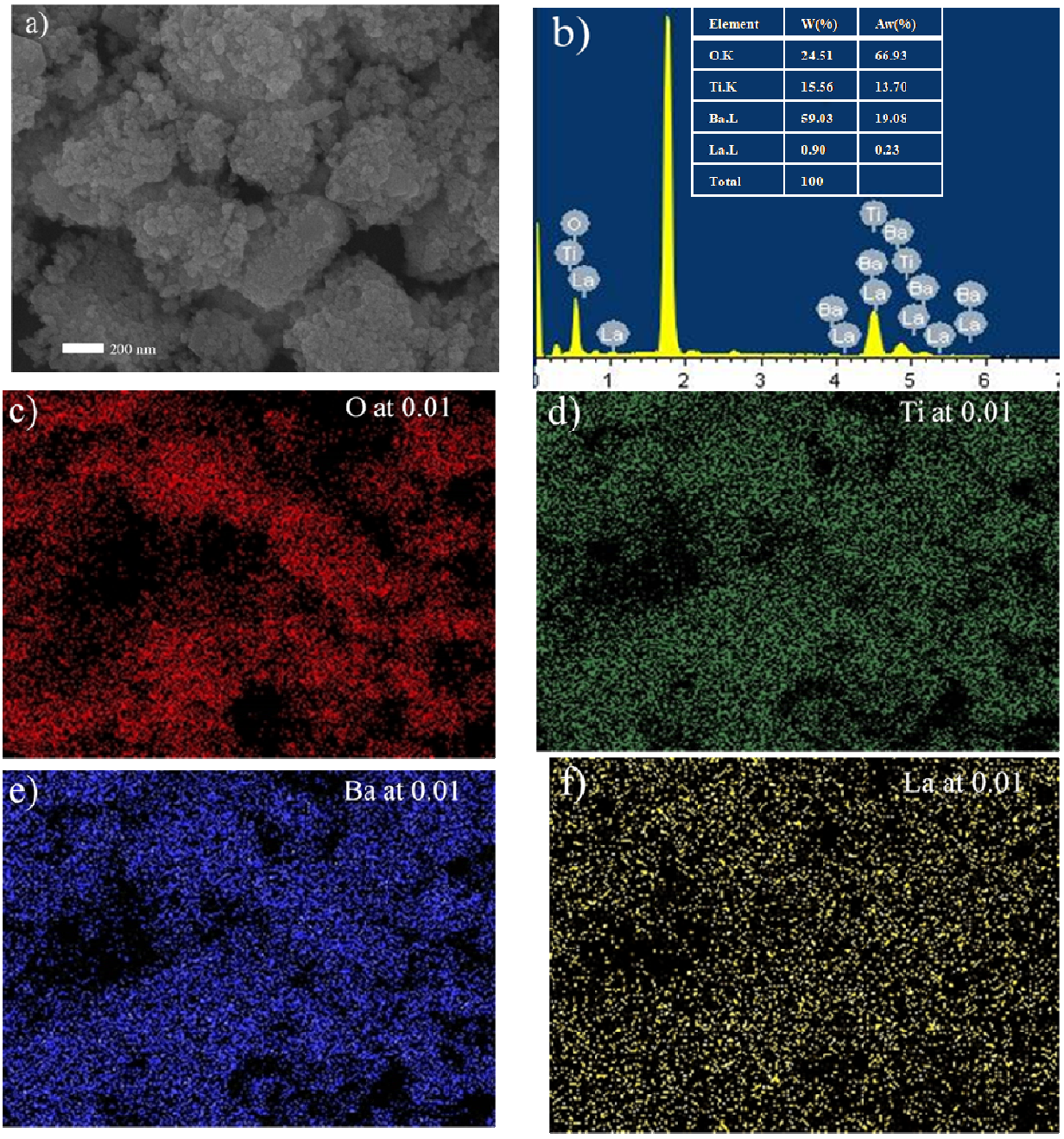

Figure 5.3 Result of $Ba_{(1-x)}TiO_3$: x La at x=0.01 (a) SEM images, (b) EDS result, (c) (d) (e)and (f) EDS mapping image of O,Ti ,Ba and La respectively.

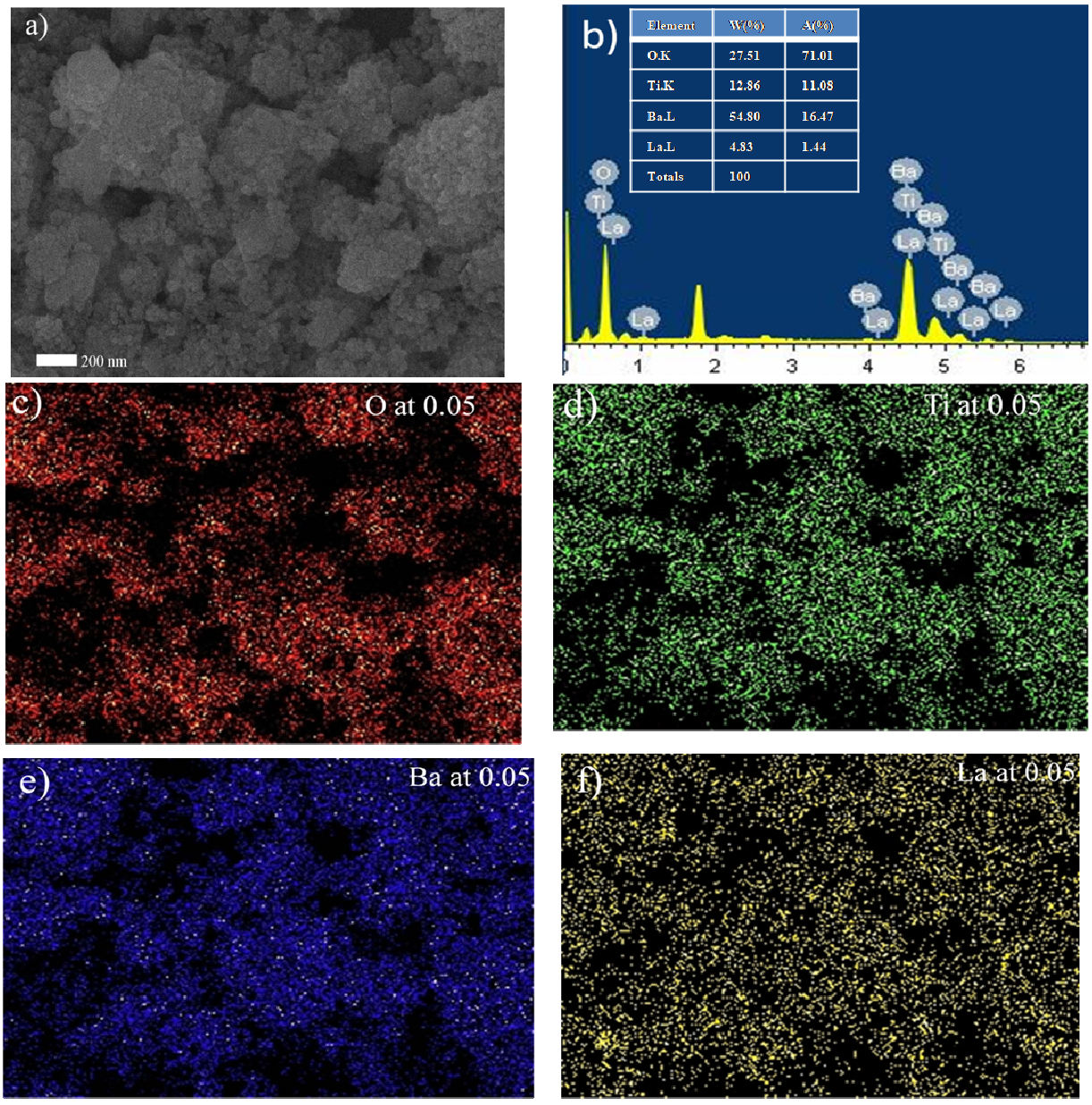

Figure 5.4Result of $Ba_{(1-x)}TiO_3$: x La at x=0.05 (a) SEM images, (b) EDS result , (c) (d) (e) and (f) EDS mapping image of O,Ti ,Ba and La respectively.

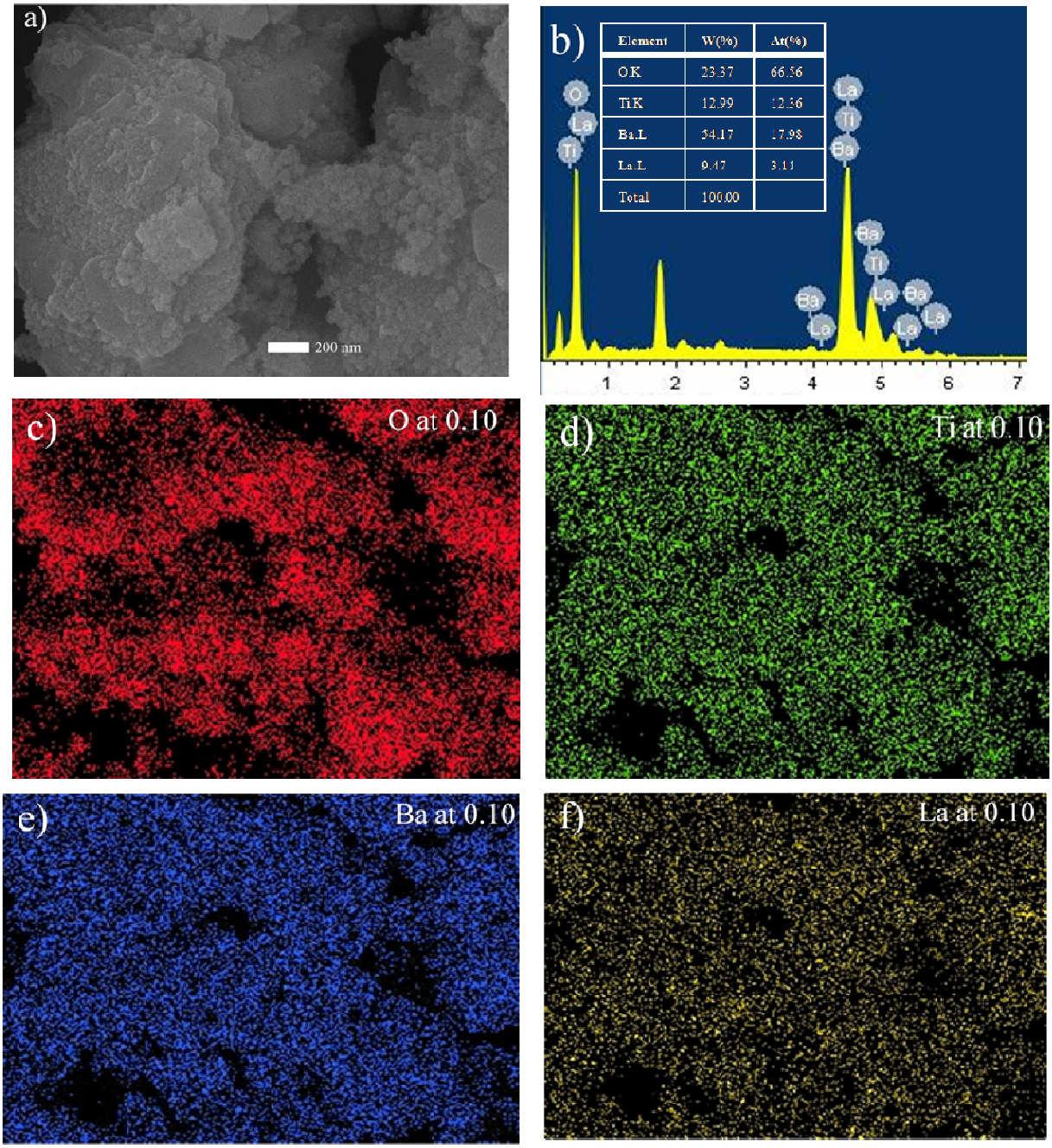

Figure 5.5 $Ba_{(1-x)}TiO_3$: x La at x=0.10 (a) SEM images, (b) EDS result, (c-f) EDS mapping of O, Ti, Ba, and La, respectively.

Electron microscopy is important instrument for double checking XRD based microstructure analysis[51]. Whereas in this work according to the result obtained from Electron scanning microscopy (SEM) as shown on Figure 5.3 to Figure 5.6.

From SEM-mapping, as showed on the bar scale (Figure 5.3a to Figure 5.6a) the estimated average grain size was found to be similar to those calculated applying Scherer's formula (table 5.2) for the same compounds. This indicates that the actual grain size in the material is similar with that detected on the surface morphology. We can also observe that, SEM images show the samples are somehow agglomerated nanoparticles (Figure5.3. a , Figure 5.4. a, Figure 5.5.a. and Figure 5.6.a).In the SEM images backscattered electron displays compositional distribution contrast which results from different atomic number elements and their distribution.

EDS analysis involves invention of an X-ray spectrum from the whole scanning area of the SEM. As shown above on Figure 5.3-5.6, image of Ba $_{(1-x)}$ TiO_3: x La as prepared sample and the related X-ray spectra which was processed from the complete scan area plotted on y-axis and X-axis. The Y-axis and the X-axis shows number of X-rays received and processed by the detector counted and the energy level of those counts respectively.

The formation of $BaTiO_3$ phase was justified by previous analysis. But, doping of activator i.e., La^{3+} in host lattice was confirmed by EDS mapping. An element image is a mapping survey of the sample materials surface captured using the electron detectors, which is colored according to the sample composition. From SEM-EDS mapping images, the result conforms an evenly distribution or allocation of composition elements of host lattice which is Ba, Ti, O where x = 0.00, and at X = 0.01, 0.05, and 0.10. Elements of host lattice are Ba, Ti, O and dopant La.

Using Energy Dispersive Spectroscopy (EDS) the particular elements distribution and their comparative proportions (Wight % and Atomic %) were identified. From EDS mapping examinations for random spots in the sample was confirmed and the material was consistently distributed while compared to the composition of each Ba $_{(x-1)}$xLa TiO_3 (x= 0.00, 0.01, 0.05, 0.10) compositions. In addition the Wight percentage of the element observed in the elemental analysis is similar amount with the amount of precursors in which weighed during synthesis (x=0.00, x=0.01, x=0.05 and x=0.10 , x= amount of La doped) and at x = 0.00 the weight

percentage of prepared (specimen) $BaTiO_3$ distribution is similar while compared with the standard data ICDD 00-031-0174 which is fitted during X-ray Characterization .

c. Raman spectroscopy

Raman spectroscopy is a powerful characterization technique in materials science, because the vibrational dynamics gives rich information on the molecular structure. Furthermore, it is a nondestructive technique and simple analysis of the data.

The Raman spectra of $Ba_{(x-1)}$ $xLaTiO_3$ obtained by WASSR at different amount of La are presented in Figure 5.7.

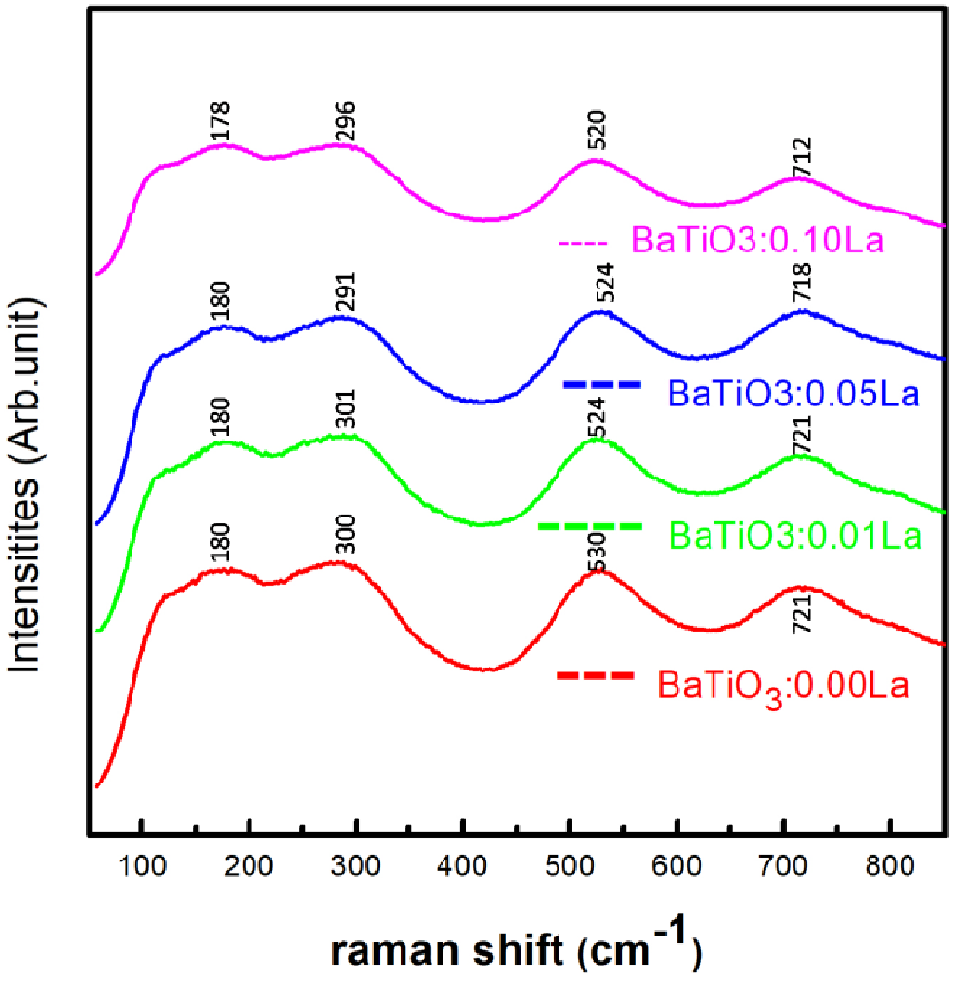

Figure 5.6 Raman spectra of $Ba_{(1-x)}TiO_3$:xLa samples at various x values

In a given propagation direction there will be polarization mode and it creates two branches, this are acoustical and optical branches longitudinal LA and transverse TA acoustical modes, and longitudinal LO and transverse TO optical modes.

Forρ atoms in the primitive cell, we have 3acoustical and 3ρ-3 optical branches. For ρ atoms and N primitive cell, we will getρN atoms. On each of the x,y,z directions individual atom has three degrees of freedom, making a total of 3ρN degrees of freedom for a crystal.[52]Therefore,$BaTiO_3$ has five atoms and fifteen degrees of freedom per unit cell.

According the crystallography, Raman-active modes for tetragonal $BaTiO_3$ has P4mm symmetry. The x-ray data show that the as prepared material ($Ba_{(x-1)}La_xTiO_3$) does not contain other than Barium Titanium Oxide ($BaTiO_3$) at x =0.00 but at x =0.01,0.05 and 0.10 the phase shows peaks for $Ba_2Ti_2O_5$in addition the intensity peaks of $Ba_2Ti_2O_5$(around 110cm^{-1}) increases with respect increasing doping amount of La.

Frequencies near to 180, 300,530and 721 $cm^{-1}$are shown in Figure 5.7.The 180 cm^{-1} and the 530 cm^{-1} mode come from cubic phase modes but the peak around 720 is from tetragonal. Many researchers have an opinion that the Raman mode around 303 cm^{-1} is a fingerprint of the tetragonal $BaTiO_3$. However, in Ba $_{(x-1)}$ $xLaTiO_3$ nanoparticles these peak positions change a little due to the strain in the structure because of the small size. This is especially evident in the crystalline peak, with the peak shifting to smaller wave numbers for nano-scaled particles. [53]

d. **UV-Vis spectroscopy Optical Analysis**

Band gap is the most crucial factor with respect to the electrical property of the materials. Figure 5.8 shows the UV–Visible spectroscopy of $Ba_{(1-x)}xLaTiO_3$. It can be seen that the minimum absorption peak of $Ba_{(1-x)}xLaTiO_3$ was found around λ of 656 nm and the related intensity values are 1.06 % at x=0. 00, 0.85% at x=0.01, 0.96% at x=0.05 and 1.35 at x=0.10%. UV-Vis spectra shows that the minimum absorption occurs when the dopant level is 1 % (x= 0.01). Thus, it can be easily deduced that the maximum reflectance was achieved when the dopant level is 1 % (x= 0.01).

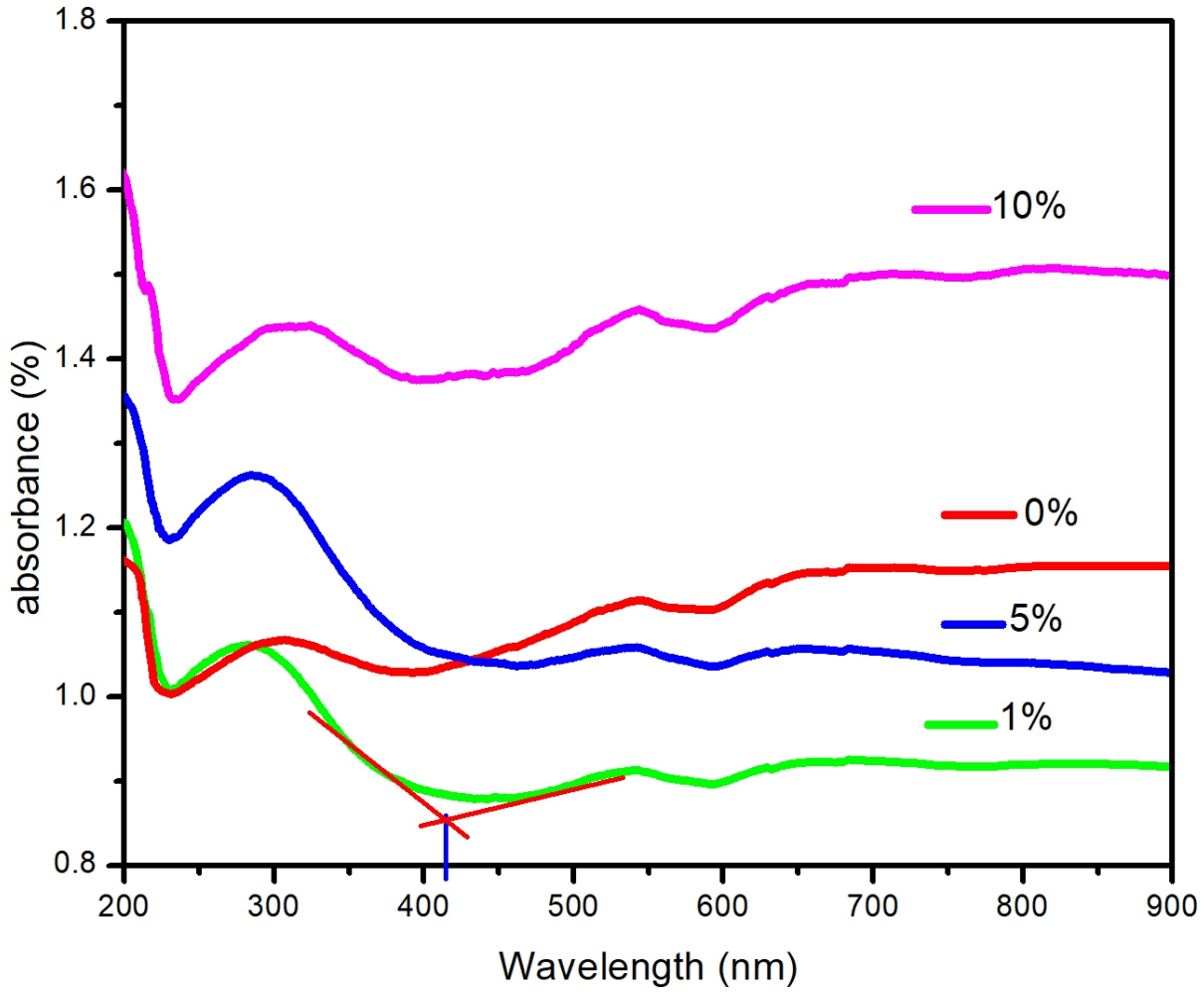

Figure 5.7 UV–Vis absorption spectra $Ba_{(1-x)}xLaTiO_3$ at x=0.00,0.01,0.05 and 0.10

The optical absorption is nearly constant in the region between 656 nm and 900 nm for $BaTiO_3$ and doped (La) atoms. Furthermore, at the range of the Visible light, $Ba_{(1-x)}xLaTiO_3$ has lower absorption at x=0.01. And also it is observed that the absorption edge of $Ba_{(1-x)}xLaTiO_3$ was found to be ca. 415 nm at x=0.01. Figure 5.9 shows the absorption edge of $Ba_{(1-x)}xLaTiO_3$at x=0.01. Using Figure 5.9 and equation 5.2 [54] , the band gap energy was calculated to be 2.99 eV This result clearly suggest that the $Ba_{(1-x)}xLaTiO_3$ can perform efficiently as a retro-reflective under Visible light; hence refractive index is closely associated to its electronic band gap.

Eg = 1240/λ, where λ is the onset absorption wavelength…….. (5.2)

Usually, the electrostatic refractive index of a semiconductor decreases with the increasing energy gap. This correlation can be understood from the following argument, suggested by Moss. [55] The energy needed to ionize the atom and to raise an electron to the conduction band scales as $Eg \sim 1/\varepsilon^2$, where ε is the background permittivity of the semiconductor. The very simple approximation for the static refractive index is known as the Moss relation (equation 5.3).

$n^4Eg = 95$ eV …… (5.3)

Where n is refractive index and Eg is band gap energy

By substituting the obtained band gap energy at ca. 415 nm (Eg = 2.99 eV) in Moss formula, the refractive index of the as prepared material (at x= 0.010 was found to be 2.392.

Commercial retro-reflective glass beads usually vary in index from around 1.5 for road markings and 1.9 for airports. Recently X. Li et al. successfully characterized $La_4Ti_9O_{24}$ (LTO) by flame-sprayed method and the measured refractive index was 2.3. [1] X. Li et al concluded that LTO is a material which is having a high reflective index. During preparation the inlet and outlet temperatures of flame-sprayer were maintained at 190 °C and 120 °C. In addition, the flame-sprayed microspheres were thermally annealed at 500 °C for 12 hours after washing. Moreover, the spray-dried powders were oven-dried and then fed into a C_2H_2-O_2 flame (>3000 °C). Thus, the high operating temperature used in flame-sprayed method makes the product expensive compared to the method used in this study, WASSR. Though simplistic approach and low temperature was employed in this study, the measured refractive index was very high, 2.392, compared to flame-sprayed method.

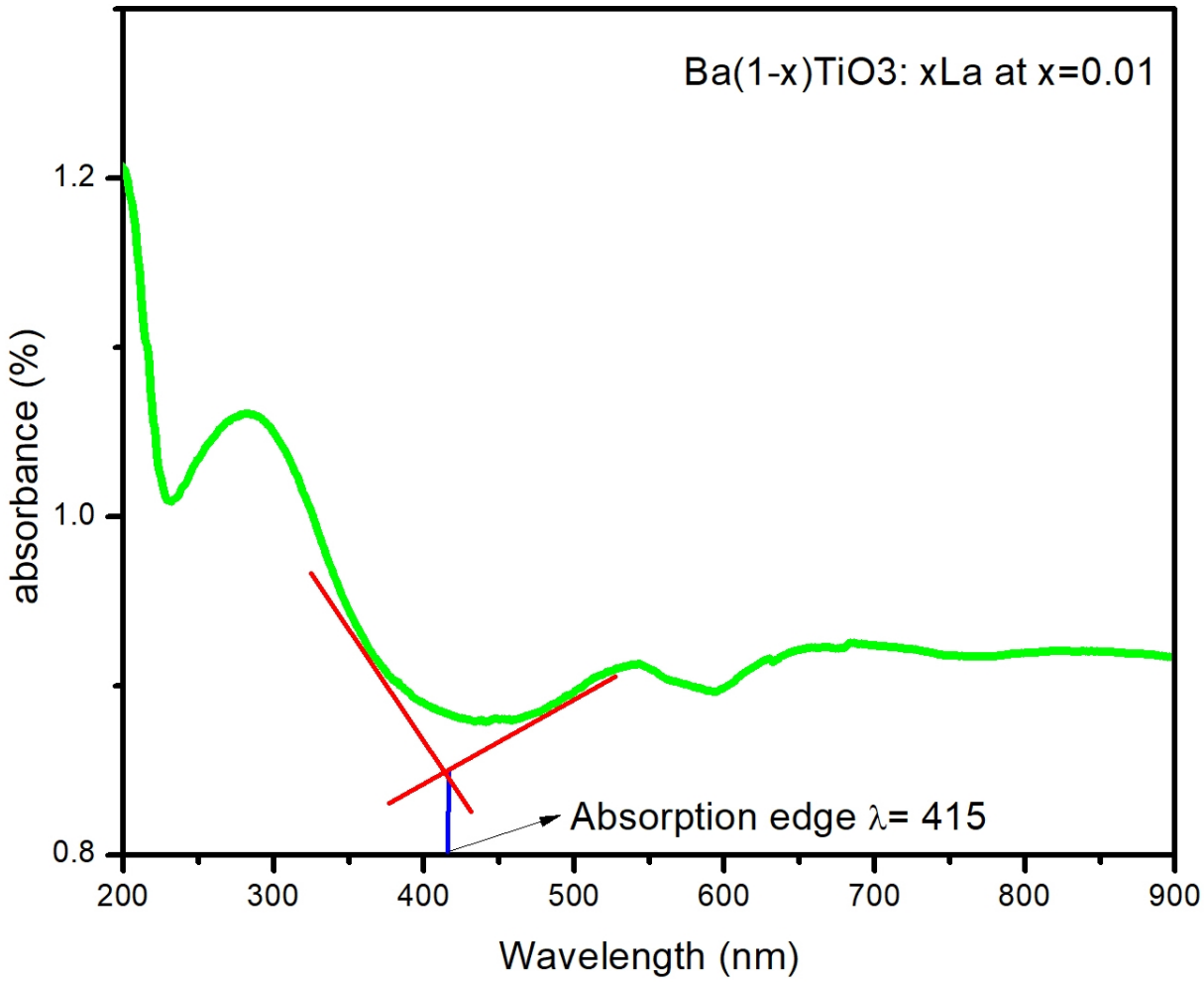

Figure 5. 8 Absorbance edge of $Ba_{(1-x)}xLaTiO_3$ at x=0.01

Using equation 5.4, 5.5 and 5.6, it is possible to calculate reflectance (R) values.

$A=\log_{10}{}^{1/T[56]}$ ..... (5.4).

$T = \frac{1}{10^A}$ ..... (5.5)

A+T+R=100% or R= 100%-A-T ..... (5.6)

Where R is reflectance, A is absorbance, and T is transmittance.

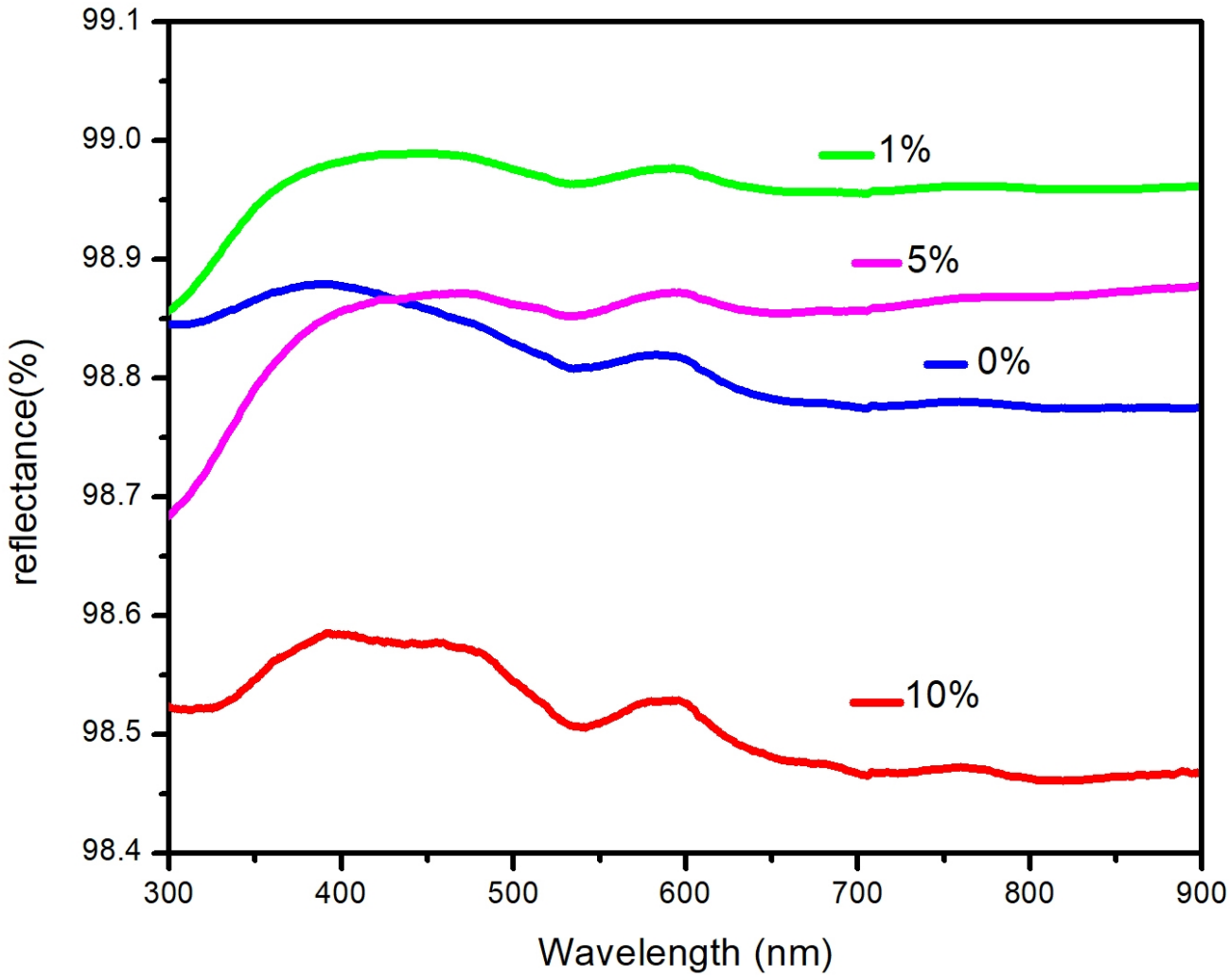

Figure 5. 9 Reflectance of $Ba_{(1-x)}xLaTiO_3$

Figure 5.10 shows reflectance values of $Ba_{(1-x)}xLaTiO_3$. It can be observed from Figure 5.10 that the reflectance values at dopant level of 0.01, 0.05, 0.00 and 0.10 were 98.99%, 98.87%, 98.76% and 98.5%, respectively, for the visible light above 428 nm. The highest reflectance was obtained at 0.01, 98.99%. Furthermore, it is observed that $BaTiO_3$ without doping and activated with La shows almost nearly equal percentage of reflectance values. However, materials shall be so effective in enhancing nighttime and daytime roadway safety that traffic signs and personal safety garments are required to be retro-reflective. Fluorescent safety colors greatly increase the daytime brightness and color contrast of signs and personal safety markings within the roadway environment.[3] Therefore, $BaTiO_3$ activated with La could increase the daytime brightness do to the fluorescent properties of La.

6. Conclusion and Recommendation.

6.1. Conclusion

Tetragonal $Ba_{(1-x)}xLaTiO_3$ nanoparticles were successfully synthesized by WASSR route using TiO_2, $Ba(OH)_2.8H_2O$ and La_2O_3 as starting materials and retro-reflective activity was evaluated under visible light. The structural, morphological and optical properties of the as prepared $Ba_{(1-x)}xLaTiO_3$ was characterized by powder XRD, SEM, EDS, Raman spectroscopy, and UV-Vis spectrometry. It is noted that Lanthanum-ions substitute successfully on the Barium sites of $BaTiO_3$ and the average grain size of $Ba_{(1-x)}$ $xLaTiO_3$ was found to be in between 19.39 to 21.64 nm. The $Ba_{(1-x)}xLaTiO_3$ nanoparticles exhibited significant photocatalytic activity under visible light irradiation. This significant photocatalytic activity of $Ba_{(1-x)}xLaTiO_3$ under visible light is mainly attributed to the special morphology and phase purity at La doping level of 1 %. The refractive index of $Ba_{(1-x)}xLaTiO_3$ using WASSR route showed a better refractive index of 2.392 at visible range than other methods such as flame-sprayed method, n = 2.3. Moreover, the $Ba_{(1-x)}xLaTiO_3$ nanoparticles prepared by using WASSR route displayed a very high refractive index, n = 2.392, nearly similar with the theoretical refractive index of $BaTiO_3$, n = 2.4, though a very simple and very low temperature were employed in the WASSR route. The observed results confirmed that the synthesized $BaTiO_3$:0.01La nanoparticles can be a potential retro-reflective material under visible light.

6.2. Recommendation

Retro-reflective materials promote the safety of vehicles, roads and people. In addition, the construction workers and first aid personnel rely on the daytime luminescence effect of the reflective belt and the night light effect to ensure their personal safety. Therefore, the material synthesized in this study has superior results to fulfill these needs. The superior results obtained and the recommended applications of the as prepared product are given below.

1. The refractive index obtained from $BaTiO_3$:xLa at x=0.01 is high (2.392) and the product can be applied in road markings, road side signs, protective reflective helmet or clothes, and heat-reflecting layers. Thus, future studies should extend to investigate the property

of $BaTiO_3$:xLa on its application areas by controlling nanoparticles size and performing field tests.

2. More studies on the synthesis of retro-reflective materials other than $BaTiO_3$:xLa using WASSR method are recommended.
3. WASSR synthesis method is easy and does not need complicated technologies. It also employs low temperature of production and small heating time making products economical. Hence, feasibility studies on industrial production of retro-reflective materials through WASSR method are recommended.

References

1. Li, X., et al., Synthesis of amorphous La $_4$ Ti $_9$ O $_{24}$ microspheres with high-refractive index via containerless flame-spraying method. Materials Research Bulletin, 2018. **97**: p. 567-571.

2. Tsao, K.Y., et al., Self-Assembled Hierarchical Arrays for Colored Retroreflective Coatings. Langmuir, 2016. **32**(48): p. 12869-12875.

3. Donahue, D.M.B.a.T.J. Measurement issues in the Color Specification of Fluorescent-Retroreflective Materials for High Visibility Traffic Signing and Personal Safety Applications. in Fourth Oxford Conference on Spectroscopy, Art Springsteen, Michael Pointer,. 2003. http://proceedings.spiedigitallibrary.org/ on 06/21/2016.

4. Grosges, T., *Retro-reflection of glass beads for traffic road stripe paints.* Optical Materials, 2008. **30**(10): p. 1549-1554.

5. Toda, K., et al., Synthesis of Nano-Sized Materials Using Novel Water Assisted Solid State Reaction Method. Key Engineering Materials, 2018. **777**: p. 163-167.

6. Humayoun, U.B., et al., Novel and Incredibly Facile Low Temperature Solid State Route to Nano-Sized Eu3+ Activated BaTiO3 Phosphors. Science of Advanced Materials, 2018. **10**(9): p. 1225-1229.

7. Darko Babic, *Evaluation of road markings retoreflection measuring methods.* European Scientific Journal F, 2014. **3**: p. 10.

8. Bagot, K.W., *Evaluation of Retro-Reflective Beads in Airport Pavement markings*. 1994, U,S. Department of Transportalion FederalAviationAdministration: Virginia. p. 65.

9. Agota Berces, S.R., Keeping people safer through better visibility Advances in retroreflective technologies for road signage, pavement markings and vehicle visibility delivering safer roads, in Australasian Road Safety Research, Policing and Education 2012, 3M Traffic Safety Systems Division: Wellington, New Zealand. p. 12.

10. Administration, F.H., *Manual on Uniform Traffic Control Devices*. 2009, Department of Transportation: Washington D.C. p. 864 `.

11. Brich, S.C., Retroreflective sign sheeting specification for fluorescent orange construction and maintenance signs October 2002 Virginia Transportation Research Council Charlottesville, Virginia

12. Hong Hua, C.G., and Jannick P.Rolland, Study of Imaging properties of Retro-reflective Materials used in Head-Mounted Projective Displays (HMPDs). 2002. **4711(2002)**: p. 8.

13. Smadi, O., et al., Predicting the Initial Retroreflectivity of Pavement Markings from Glass Bead Quality. 2013.

14. Sheikh Azhar U Rehman, A.K.D., *Comparative Analysis of Pavement Marking Material based on Retro-Reflectivity.* International Research Journal of Engineering and Technology, 2015: p. 12.

15. Mario Aparicio, A.J., Lisa Klein, *Handbook of Sol-Gel Science and Technology*. Second Edition ed, ed. M.A. Lisa Klein , Andrei Jitianu. 2005. 3754.

16. harles E. Searight, E.M.A., and John R.Ryan, Jackson, Miss,, *Hgh index of refraction glass compositions.* United States Patent Office, 1968. **3,419,403**: p. 8.

17. Gao, L.H., Z. Ma, and Q.B. Fan, First-principle studies of the electronic structure and reflectivity of LaTiO3 and Sr doped LaTiO3 (La1-xSrxTiO3). Journal of Electroceramics, 2011. **27**(3-4): p. 114-119.

18. John D. Bullough, N.P.S., Conan P. O'Rourke, *LEGIBILITY OF URBAN HIGHWAY TRAFFIC SIGNS USING NEW RETROREFLECTIVE MATERIALS.* Lighting Research Center, Rensselaer Polytechnic Institute, 21 Union St., Troy, NY 12180 USA, 2010. **25**(accepted 19 July 2010): p. 8.

19. Kostromitin, K.I., *Technological Aspects of the Retroreflective Sheeting Production.* Procedia Engineering, 2016. **150**: p. 1046-1049.

20. AZoM, Barium Titanate (BaTiO3) Properties and Applications. 2004.

21. Donegá, C.d.M., *Nanoparticles Workhorses of Nanoscience*, ed. C.d.M. Donegá. 2014, Netherlands: Springer.

22. Kim SW, A.Y., Watanabe M, Hasegawa T, Muto M, Toda A, Ishigaki T, Uematsu K, Toda K, Sato M, Kawakami E, Koide J, Toda M, Kudo Y, Masui T, Masaki T, Yoon DH, *Yellow MgV2O6·2H2O nanophosphor synthesized by a water-assisted solid-state reaction (WASSR) method at low temperature below 80 °C ,Dyes and Pigments (2017)*. 2017. p. 27.

23. GALASSO, F.S., *Inorganic Syntheses Barium Titanate, BaTi03* 2007: United Aircraft Research Laboratories, East Hartford, Conn. 06108. . 2.

24. Roy, A.S.B.R.G.R. The perovskite structure – a review of its role in ceramic science and technology. 2000. 24.

25. Pfaff, G., *BaTiO3 Preparation by Reaction Ba(OH)2* 1991, England: Elsevier Science Publishers Ltd. 5.

26. Mingmei Wu, J.L., Guangguo Wang, Aihong Huang, and Yuji Luo Hydrothermal Synthesis of Tetragonal Barium Titanate from Barium Hydroxide and Titanium Dioxide under Moderate Conditions. 1999: p. 3.

27. Grande, M.-A.E.a.T., *1D oxide nanostructures from chemical solutions*. 2014: Chem. Soc. Rev.

28. Zhu, X., et al., Atomic-Scale Characterization of Barium Titanate Powders Formed by the Hydrothermal Process. Journal of the American Ceramic Society, 2008. **91**(3): p. 1002-1008.

29. Mohamed.N..Rahaman, Ceramic Processing and Sintering-M. Dekker . 2003.

30. Cernea, M., Sol-gel synthesis and characterization of $BaTiO_3$ Powder. 2005: p. 8.

31. KAREIVA, A., *Sol-gel synthesis and characterization of barium titanate powders.* Journal of materials science, 1999. **34**(23 March 1999): p. 4853-4857.

32. B. Lee, J.Z., Preparation, structure evolution and dielectric properties of $BaTiO_3$ thin films and powders by an aqueous sol-gel process. Elsevier, 2001. **388**: p. 107-113.

33. Simon-Seveyrat, L., Re-investigation of synthesis of BaTiO3 by conventional solid-state reaction and oxalate coprecipitation route for piezoelectric applications. 2005, 69621 Villeurbanne Cedex, France: Elsevier.

34. Kim, S.W., et al., Nanophosphors synthesized by the water-assisted solid-state reaction (WASSR) method: Luminescence properties and reaction mechanism of the WASSR method. Applied Spectroscopy Reviews, 2017. **53**(2-4): p. 177-194.

35. Sun Woog Kim, T.H., Mizuki Watanabe, Kazuma Sugimoto, Yu Saito, Kazuyoshi Uematsu, Kenji Toda, Mineo Sato, *Environmentally friendly Rb3V5O14 fluorescent red pigment*, N.U. Graduate School of Science and Technology, 8050 Ikarashi 2-nocho, and J. Niigata 950-2181, Editors. 2016. p. 24.

36. Kenji Toda1, a., Sun Woog Kim1, Takuya Hasegawa1, Mizuki Watanabe1, Tatsuro Kaneko1, Ayano Toda1, Atsushi Itadani1, Mineo Sato2, Kazuyoshi Uematsu2, Tadashi Ishigaki1, Junko Koide3, Masako Toda3, Yoshiaki Kudo3, Takaki Masaki4 and Dae Ho Yoon4, *Novel Soft Chemical Synthesis Methods of Ceramic Materials* 2016, Switzerland: Trans Tech Publications. 4.

37. Kenji Toda1, a., Sun Woog Kim1, Takuya Hasegawa1, Mizuki Watanabe1, Tatsuro Kaneko1, Ayano Toda1, Ryota Yamanashi1, Shota Kumagai1, Masaru Muto1, Atsushi Itadani1, Mineo Sato2, Kazuyoshi Uematsu2, Tadashi Ishigaki1, Junko Koide3, Masako Toda3, Emiko Kawakami3, Yoshiaki Kudo3, Takaki Masaki4 and Dae Ho Yoon4,b* *Development of Water Assisted Solid State Reaction for the Ceramic Materials* 2017, Switzerland: Trans Tech Publications. 5.

38. Kenji Toda1*, T.K., Takuya Hasegawa1, Mizuki Watanabe1,Yusuke Abe1, Takeshi Kuroi1, Mineo Sato1, Kazuyoshi Uematsu1, *Synthesis of Nano-Sized Materials Using Novel Water Assisted Solid State Reaction Method* 2018, United Kingdom-10/09/18,01:49:56): Trans Tech Publications,. 5.

39. Mizuki WATANABE, J.I. *Synthesis of Li2SiO3 using novel water-assisted solid state reaction method*. 2017. 4 DOI: http://doi.org/10.2109/jcersj2.16325.

40. Hasegawa, T. Determination of the crystal structure and photoluminescence properties of $NaEu_{1-x}Gdx(MoO4)2$ phosphor synthesized by a water-assisted low-temperature synthesis technique. =, 2017. 25089–25094 DOI: 10.1039/c7ra01832k.

41. Toda, K., et al., Development of Water Assisted Solid State Reaction for the Ceramic Materials. Key Engineering Materials, 2017. **751**: p. 353-357.

42. Mourdikoudis, S.P., R. M.Thanh, N. T. K., Characterization techniques for nanoparticles: comparison and complementarity upon studying nanoparticle properties. Nanoscale, 2018. **10**(27): p. 12871-12934.

43. Ai, L., Nanoscale Zerovalent Iron Particles for Environmental Restoration, ed. T.P.G.V. Lowry. 2019, Switzerland: Springer

44. Scimeca, M.B., S. Lamsira, H. K. Bonfiglio, R. Bonanno, E., *Energy Dispersive X-ray (EDX) microanalysis: A powerful tool in biomedical research and diagnosis.* Eur J Histochem, 2018. **62**(1): p. 2841.

45. Zhang, J.Z., *Optical properties and spectroscopy of nanomaterials*. 2008, 5 Toh Tuck Link, Singapore 596224: World Scientific Publishing Co. Pte. Ltd.

46. Thompson, C., Barium titanate: The relationship between the conditions of synthesis and its structural and electrical properties, in Chemistry. May 1996.

47. Waseda, Y., X-Ray Diffraction Crystallography_ Introduction, Examples and Solved Problems. January 2011, Sendai, Japan: Springer.

48. Stojanovic, B.D., *Mechanochemical synthesis of ceramic powders with perovskite structure.* Journal of Materials Processing Technology, 2003. **143-144**: p. 78-81.

49. Suzuki, N., Osada, M., Billah, M., Bando, Y., Yamauchi, Y., Hossain, S.A, chemical-synthesis-porous-barium-titanate-thin-film and Thermal Stabilization of Ferroelectric Phase by Porosity-Induced Strain. 2018.

50. Stock, B.D.C.S.R., Elements of X-Ray Diffraction-Pearson Education Limited 2014: p. 654.

51. (Eds.), E.J.M.P.S., *Diffraction Analysis of the Microstructure of Materials* Springer Series in Materials Science 2004. **68** p. 554.

52. Kitte, C., *Introduction to Solid State Physics-Wiley (2005).* Vol. 703. 2005, United states of America: John Wiley & Sons ,Inc.

53. Garg, P., Study of Photoluminescence from Amorphous and Crystalline Silicon Nanoparticles. 2015, Arizona state university: Yong Hang Zhang. p. 85.

54. Ghobadi, N., *Band gap determination using absorption spectrum fitting procedure.* Springeropen journal, 2013. **International Nano Letters 2013 3:2.**

55. Moss, T.S., Relations between the Refractive Index and Energy Gap of Semiconductors. 1985: p. 13.

56. Mayerhofer, T.G.M., H.Popp, J., Employing Theories Far beyond Their Limits-The Case of the (Boguer-) Beer-Lambert Law. Chemphyschem, 2016. **17**(13): p. 1948-55.